Snail1-induced partial epithelial-to-mesenchymal transition drives renal fibrosis in mice and can be targeted to reverse established disease

M. Teresa Grande[1,5,9], Berta Sánchez-Laorden[1,9], Cristina López-Blau[1], Cristina A. De Frutos[1,6], Agnès Boutet[1,7], Miguel Arévalo[2,3], R. Grant Rowe[4,8], Stephen J. Weiss[4], José M. López-Novoa[2,3] and M. Angela Nieto[1,10]

[1]Instituto de Neurociencias (CSIC-UMH), Avda. Ramón y Cajal s/n, San Juan de Alicante, Spain

[2]University of Salamanca, Campus Miguel de Unamuno, Salamanca, Spain.

[3]Biomedical Research Institute of Salamanca (IBSAL), Salamanca, Spain.

[4]Division of Molecular Medicine and Genetics, Department of Internal Medicine, Life Sciences Institute, University of Michigan, Ann Arbor, USA

Present addresses:

[5]Department of Biotechnology, Universidad Francisco de Vitoria, Pozuelo de Alarcón, Madrid, Spain

[6]Brain Development and Plasticity Group, IBENS, Inserm U1024, Avenir Team, CNRS UMR 8197. Paris, France

[7]CNRS, Sorbonne Université, UPMC Univ Paris 06, FR2424, Station Biologique, F-29688 Roscoff, France

[8]Department of Pediatric Oncology, Dana-Farber Cancer Institute, Harvard Medical School, Boston, Massachusetts 02215 USA

[9]These authors equally contributed to this work

[10]Author for correspondence: M. Angela Nieto
e-mail: anieto@umh.es
Tel: 34-965919243

Keywords: Renal fibrosis, Partial EMT, Snail, Antifibrotic therapies

Progressive kidney fibrosis contributes greatly to end-stage renal failure, and no specific treatment is available to preserve organ function. During renal fibrosis, myofibroblasts accumulate in the interstitium of the kidney leading to massive deposition of extracellular matrix and organ dysfunction. The origin of myofibroblasts is manifold and the contribution of an epithelial-to-mesenchymal transition (EMT) undergone by renal epithelial cells during kidney fibrosis is still debated. We show that the reactivation of *Snai1* in renal epithelial cells is required for the development of fibrosis in the kidney. Damage-mediated Snail1 reactivation induces a partial EMT in tubular cells that, without directly contributing to the myofibroblast population, relays signals to the interstitium to promote myofibroblast differentiation and fibrogenesis and to sustain inflammation. We also show that Snail1-induced fibrosis can be reversed *in vivo* and that obstructive nephropathy can be therapeutically ameliorated in mice by Snail1 inhibition. These results reconcile conflicting data on the role of EMT in renal fibrosis and provide avenues for the design of novel anti-fibrotic therapies.

Kidney fibrosis is a hallmark of chronic kidney disease (CKD), the progressive deterioration of kidney function, which leads to end-stage renal failure[1]. The only treatment available is the replacement of renal function by dialysis or kidney transplantation, which represented in 2009 a cost of over $40 billion in the United States[2]. CKD is characterized by glomerulosclerosis and tubulo-interstitial fibrosis, regardless of the initial cause of the renal disease. The development of the renal system involves several rounds of epithelial-to-

mesenchymal and mesenchymal-to-epithelial transitions (EMTs and METs, respectively[3]). *Snai1*, which encodes the transcription factor Snail1, a potent EMT inducer during embryonic development and tumor progression[4], is expressed in the precursors of the renal epithelial cells. But its expression is downregulated upon epithelial differentiation and maintained in a silent state during adulthood[5] as the suppression of epithelial plasticity is crucial to maintain normal tissue architecture and homeostasis. We previously showed that activation of Snail1 in renal epithelial cells leads to renal fibrosis and renal failure in an inducible transgenic mouse model (Snail1-ERT2)[5]. Snail1 is also reactivated in mice subjected to unilateral ureteral obstruction (UUO)[6,7,8], a standard model for progressive renal fibrosis[9] and in fibrotic lesions obtained from patients subjected to nephrectomy[5]. Thus, Snail1 reactivation in adult kidneys is sufficient to induce renal fibrosis and kidney fibrosis is associated with Snail1 activation in animal models and in patients. However, those observations do not address the question of whether Snail1 reactivation, and in turn, an EMT-like program is required for renal fibrosis to develop. While initial cell fate tracing experiments described a significant contribution of renal epithelial cells to myofibroblasts[10], subsequent studies could not find labeled epithelial cells within the interstitium in animal models of renal fibrosis[11,12,13]. Here, we directly assessed the role of Snail1 and EMT and show that the reactivation of Snail1 is not only sufficient but also required for the development of kidney fibrosis. We show that Snail1 reactivation in renal epithelial cells triggers a partial EMT that, without directly generating interstitial myofibroblasts, relays crucial signals for the differentiation of myofibroblasts and markedly contributes to the inflammatory response. The partial EMT program leads to

dedifferentiation of renal epithelial cells and promotes kidney fibrosis but preserves the integrity of the renal tubules. Here we show that the fibrosis response can be reversed *in vivo* by inhibition of Snail1 expression in mouse models of kidney injury.

RESULTS

Snail1 depletion ameliorates UUO-induced fibrosis

To directly assess the contribution of Snail1 reactivation in epithelial cells to renal fibrosis, we crossed Snai1$^{fl/fl}$ mice[14] with a strain bearing the Ksp1.3-Cre transgene[15]. Ksp cadherin (Cadherin-16) is a kidney-specific cadherin expressed in renal epithelial cells both in the cortex and in the medulla. The resulting strain *Ksp1.3-Cre*; *Snai1*$^{fl/fl}$, referred to as SFKC hereafter (**Supplementary Fig. 1**), impedes Snail1 expression in Cadherin-16 positive cells. Snail1 expression is silent in the adult kidney but it is reactivated after UUO in the cortex and in the medulla (**Supplementary Fig. 1c**). During renal development, Snail1 is a strong *Cadh16* repressor[5], and it is only when *Snai1* is downregulated that renal cells express Cadherin-16 and epithelialization occurs. As Snail1 is silenced in the adult, preventing Snail1 activation in Cadherin-16 positive cells in the kidney does not have any impact in healthy mice. As expected, while Snail1 was highly reactivated in the kidney upon UUO, this was not the case in recombined renal epithelial cells in SFKC mice (**Fig. 1a-c**). We analyzed overall morphology, collagen deposition and expression of alpha smooth muscle actin (α-SMA) and vimentin 7 or 15 days after UUO and found that kidneys from SFKC mice were protected from the development of overt fibrosis, although signs of tubular distension resulting from the obstruction

were readily evident (**Fig. 1d**,**e** and **Supplementary Fig. 2a**,**b**). We confirmed the attenuation of fibrosis by analysis of the expression of epithelial and mesenchymal markers and this was particularly evident 2 weeks after UUO (**Fig. 1f**)**.** Quantification of Sirius Red staining (**Fig. 1g**) showed a 35% reduction in fibrosis in the cortex of obstructed kidneys from SFKC mice when compared to obstructed kidneys from WT or control (Ksp1.3-Cre-only) mice (**Fig. 1g** and **Supplementary Fig. 3a**,**b)**. In our SFKC model, Snail1 reactivation was also prevented in the collecting ducts, and we observed a much better preserved morphology and lower collagen deposition in the medulla compared to WT animals (**Supplementary Fig. 3c**) indicating that the overall protection from fibrotic degeneration is higher than that reflected by the quantification of Sirius Red in the cortex.

We next assessed the contribution of epithelial cells to the interstitium after UOO in our system. We generated a mouse model harboring *Cre-loxP* mediated expression of the Tomato fluorescent protein driven by the *Ksp 1.3* promoter (Ksp1.3-Cre; Rosa-LSL-TdTomato). These mice allow the visualization and fate mapping of renal epithelial cells. Notably, we could not detect tdTomato+ cells in the interstitium 7 days after obstruction (**Supplementary Fig. 4a**) and found less than 1% after 15 days (**Fig. 2a**). One of those rare cells leaving the tubule is shown in **Supplementary Fig. 4b**. Thus, renal epithelial cells do not delaminate from the tubules to contribute to myofibroblasts or other interstitial cells, also in keeping with the observation that the total number of tubular cross sections did not differ between kidneys from WT or SFKC mice 15 days after UUO (**Fig. 2b**), indicative of tubular integrity.

Snail1 expression was reactivated after UUO in over 80% of tubular cells and also in activated interstitial cells as reported in cancer models[16] (**Fig. 2c**).

Although tubular cells did not significantly contribute to myofibroblasts, UUO provoked the downregulation of the epithelial markers *Cadh1* and *Cadh16* (**Fig. 1f**) together with the loss of polarity/differentiation as seen by the disappearance of lectin expression[17] in renal epithelial cells that have reactivated Snail1 (**Fig. 2a**,**d**). Fifteen days after UUO, some epithelial cells (around 30%) also activated the expression of α-SMA (**Fig. 2a**) and the Collagen I gene (**Supplementary 4c**), the latter a downstream target of Snail1 in the kidney[5].

Our data indicate that after renal injury the tubular epithelial cells, in spite of Snail1 reactivation, continue to display integration into the tubular tissue. Therefore, it seems that UUO-induced Snail reactivation triggers only a partial EMT in both cortical and medullar renal epithelial cells which do not acquire an invasive phenotype but that leads to damaged tubules and collecting ducts. As all of this is highly attenuated in the kidneys from SFKC mice in which epithelial cells cannot reactivate Snail1 expression (**Fig. 1**, **Fig. 2d** and **Supplementary Figs. 2b**, **4**, **5d**), we conclude that Snail1 reactivation in renal epithelial cells has an important impact on the development of fibrosis.

Snail1 reactivation promotes fibrogenesis and inflammation

Our results indicate that damaged Snail1-expressing renal epithelial cells, while being integrated in the tubules, can send signals to the interstitium, as the α-SMA+ myofibroblast population is very much reduced in obstructed kidneys from SFKC mice (**Fig. 1e**). Injured epithelial cells produce TGF-β-

containing exosomes that promote the proliferation and activation of interstitial fibroblasts[18] and TGF-β signaling is also important for the differentiation of myofibroblasts from bone marrow-derived mesenchymal stem cells[18]. In relation to this, we found that both *Tgfb1* expression and the activation of TGF-β signaling in the obstructed kidney, measured by phospho-Smad2 staining, were dependent on Snail1 reactivation in renal epithelial cells (**Fig. 1h** and **Supplementary Fig. 5a**), compatible with the role of Snail1 as an activator of the TGF-β pathway in cancer cells[19]. Thus, the lower TGF-β signaling in obstructed kidneys from SFKC mice can explain the decrease in the α-SMA+ population (**Fig. 1e** and **Supplementary Fig. 2b**).

As TGF-β is also involved in the recruitment of macrophages[20] we examined F4/80 expression and observed that macrophage colonization in obstructed kidneys from SFKC mice was highly attenuated, as was the overall inflammatory response as indicated by the lower levels of nuclear phospho-NF-κB (pNF-κB) in tubular cells when compared to WT mice (**Fig. 3a**). Taking advantage of the *LacZ* reporter allele in our SFKC mice, we confirmed that pNF-κB labeling was absent in tubules that had recombined (X-gal-positive tubules) and therefore, are not competent to reactivate Snail1 (**Supplementary Fig. 5b**).

We next analyzed the F4/80 macrophage population and identified polarized M2 macrophages in obstructed kidneys from WT mice (CD163+; **Fig. 3a**), the macrophage type enriched in the tumor microenvironment[21]. As UUO induces a robust inflammatory response and Snail1 can induce the expression of some inflammatory cytokines[22], we compared the levels of cytokines present in obstructed kidneys. We found that the levels of a number of pro-inflammatory cytokines were lower in kidneys from SFKC mice compared to WT mice,

indicating that Snail1 reactivation in tubular cells impinges on the inflammatory response. These cytokines included TNF-α and several chemokines associated with macrophage recruitment (**Fig. 3b**). Snail1 has been shown to enhance the recruitment of M2 macrophages to the tumor site by directly activating the transcription of the *Tnfa, Ccl2* and *Ccl5* genes in tumor cells[23]. As all three are included among the cytokines present in a lower amount in the obstructed kidneys from SFKC mice, we checked their expression after UUO. *Tnfa, Ccl2* and *Ccl5 levels* were higher in the obstructed kidney with respect to the control contralateral kidneys 7 days after UUO, but *Tnfa* expression was already higher 3 days after surgery (**Fig. 3c**). When we compared WT to SFKC mice we found differences in *Ccl5* levels from 7 days after UUO and these differences were apparent for all three cytokines after 15 days (**Fig. 3c**). Thus, Snail1 reactivation is required to sustain inflammation, although the early inflammatory response seems to be Snail1-independent at least for some of the cytokines (**Fig. 3b**,**c**). Nevertheless, some of the early inflammatory responses also require Snail1 reactivation, as seen by the higher level of nuclear pNF-κB in tubular cells and the higher *Tgfb1* expression in obstructed kidneys from WT versus SFKC mice 3 days after surgery (**Fig. 3d**,**e**). Altogether these data indicate that UUO-induced fibrosis concurs with a partial EMT of renal epithelial cells mediated by the reactivation of Snail1. Tubular cells do not engage into the delamination/invasion program and therefore, do not directly contribute to interstitial fibroblasts. However, this Snail1-induced partial EMT impinges on the TGF-β and NF-κB pathways together with cytokine production to promote myofibroblast differentiation, fibrogenesis, macrophage recruitment and

sustained inflammation, all required for the development and progression of organ fibrosis.

Snail1 depletion attenuates folic acid-induced fibrosis

We extended our studies to an additional model of renal fibrosis, folic acid (FA)-induced nephropathy[24]. As expected, a single intraperitoneal injection of FA induced a patchy interstitial fibrosis from 4 weeks after injection. We detected all signs of overt fibrosis, including altered tubular morphology, loss of epithelial differentiation, a numerous myofibroblast population, excessive collagen deposition and macrophage colonization in WT mice (**Fig. 4a** and **Supplementary Fig. 6a**). Quantitative analysis of epithelial and mesenchymal markers transcripts confirmed the increase in *Snai1*, *Col1a1*, *Vim* and *Acta2* levels, and the decrease in *Cadh1 and Cadh16* levels in the kidneys of FA-treated WT mice (**Fig. 4b**).

The expression of the main fibrogenic (that is, *Tgfb1*) and inflammatory signals (that is, *Tnfa*) was also increased (**Fig. 4b**). Notably, all of these changes were highly reduced in SFKC mice (**Fig. 4** and **Supplementary Fig. 6**). The analysis of cytokines also confirmed a robust reduction in the levels of pro-inflammatory cytokines, including TNF-α, CCL2 and CCL5 in FA-treated SFKC mice vs FA-treated WT mice (**Fig. 4c**). We observed a 62% reduction in fibrosis in the cortex of these mice (**Fig. 4d**) and the medulla was also protected (**Fig. 4a** and **Supplementary Fig. 6b)** indicating that, even more pronounced than after UUO, the reactivation of Snail1 in renal epithelial cells is crucial for the development of FA-induced fibrosis.

Established fibrosis can be ameliorated *in vivo*

Embryonic and cancer cells present a high degree of epithelial plasticity in terms of EMT and its reverse process MET[25]. To examine whether some plasticity exists in fibrotic tissues, we used the renal epithelial cell-specific Snail1-ERT2 fibrosis model that we generated previously[5]. In this model, Snail1 is activated by tamoxifen-induced nuclear translocation of the protein and deactivated upon tamoxifen withdrawal (**Supplementary Fig. 7**). We first confirmed that in MDCK-Snail1-ERT2 cells treated with tamoxifen Snail1 translocated to the nucleus and that the cells underwent EMT. After tamoxifen removal and concomitant with the absence of nuclear Snail1, the cells reverted to an epithelial phenotype (**Supplementary Fig. 7**).

Next, we tested whether Snail1-induced fibrosis could be attenuated *in vivo* after the disease was established (**Fig. 5a**). In Snail1-ERT2 mice, as in cultured cells, Snail1 protein efficiently shuttled from the cytoplasm to the nucleus upon tamoxifen administration and was detected back in the cytoplasm after tamoxifen removal (**Fig. 5b**). Fibrosis developed after 8 weeks of tamoxifen exposure in the Snail1-ERT2 model when compared to WT mice (**Fig. 5** and **Supplementary Fig. 8**) as seen by histology, Sirius red staining and the expression of mesenchymal and epithelial markers detected either by immunostaining or gene expression analyses (**Fig. 5c**,**d** and **Supplementary Fig. 8a**). Snail1-induced fibrosis also concurred with the activation of *Tgfb1* expression and an increase in the inflammatory response (nuclear pNF-κB) and macrophage recruitment (**Fig. 5c**,**d**). All these features were highly attenuated with the translocation of Snail1 back to the cytoplasm 8 weeks after tamoxifen

removal. Particularly, collagen deposition, mesenchymal markers, *Tgfb1* levels and inflammation almost returned to basal levels (**Fig. 5c**,**d**). Sirius Red staining in the renal cortex showed a reversion of 56% in overall fibrosis (**Fig. 5e**) and, notably, glomerular filtration rate assessed by creatinine clearance also shifted back to normal after being decreased upon Snail1 reactivation (**Supplementary Table 1**). Plasma levels of creatinine were also compatible with this. Altogether, these data show that Snail1-induced fibrosis can be ameliorated *in vivo*.

However, this experimental design does not address whether renal fibrosis developed in response to natural stimuli including damage could also be ameliorated by inhibiting Snail1. Thus, we next therapeutically inhibited Snail1 function in the UUO model. Seven days after UUO, when mice had already developed fibrosis as shown in **Fig. 1b** and **Supplementary Fig. 2b**, we systemically injected 2 different VIVO-morpholinos designed against a splicing site in the *Snai1* mRNA (Snail1-MO1 and -MO2; **Fig. 6a**; **Supplementary Fig. 9** and Online Methods). This allowed us to assess the efficacy of the Morpholino in blocking Snail1 expression in each individual mouse, and compare this with the progression of fibrosis after testing the levels of the correctly spliced isoform and those in which exon 2 was missing (**Fig. 6** and **Supplementary Figure 9**). In **Fig. 6** we show a control mouse and mouse #5 in which the MO prevented Snail1 normal splicing (**Supplementary Fig. 9a**). In this experimental setting, Snail1 inhibition should not be restricted to the tubular cells. When we compared mice subjected to UUO for 7 days and then treated with either control morpholino (Control-MO) or Snail1-MOs, we observed that Snail1 inhibition blocked the progression of UUO-induced fibrosis. Kidneys from Snail1-MO–treated mice presented a recovered morphology, lower collagen deposition and

lower expression of vimentin and α-SMA (**Fig. 6b**). Similarly, expression analysis indicated that *Snai1*, *Snai2* and *Vim* levels were significantly lower and *Cadh1* and *Cadh16* levels higher in Snail1-MO treated mice when compared with those in obstructed kidneys from mice injected with Control-MO (**Fig. 6c**). Furthermore, as observed in our analyses of the SFKC mice, Snail1 had a marked impact on *Tgfb1* expression, macrophage colonization and inflammation (**Fig. 6b**,**c**), as all these responses were highly attenuated upon Snail1 inhibition. Further, quantification of cortical fibrosis revealed a reduction of 57% after treatment with Snail1-MO versus Control-MO (**Fig. 6d**). This attenuation is specific for Snail1 depletion as it did not occur after the injection of Snail1-MO1 in mice in which the MO did not efficiently blocked normal mRNA splicing (**Supplementary Fig. 9**). In summary, this data indicate that Snail1 inhibition can significantly attenuate established UUO-induced fibrosis in mice.

DISCUSSION

CKD can result from urinary obstruction, autoimmune disorders, unresolved inflammation or deterioration of transplants[1], progressing irreversibly to end-stage renal disease that requires dialysis or kidney transplantation. No specific therapy is available to recover organ function and the cellular mechanisms that drive interstitial fibrosis are still under debate, as conflicting results have either assigned an important or a negligible role of tubular EMT in the progression of renal fibrosis[10-13,26,27]. In addition, inflammatory cytokines and cells are major effectors of the chronic disease[20,28], but the mechanisms by which chronic inflammation impinges on fibrogenesis still remain unclear. Understanding this

link is key in the design of therapeutic strategies to halt the progression of CKD[29]. Using renal epithelial-specific mouse models, and in particular modifying Snail1 expression in medullar and cortical renal epithelial cells, we provide evidence of the contribution of EMT and the link between inflammation and fibrosis.

With respect to the EMT, we show that (i) a partial EMT of renal epithelial cells is activated upon renal damage, (ii) these damaged cells remain integrated in the tubules while relaying fibrogenic and inflammatory signals that lead to the progression of the disease, and (iii) both fibrogenesis and inflammation require the activation and maintenance of the potent EMT inducer Snail1. Therefore, our results highlight the importance of an EMT-like program in renal epithelial cells for the development of fibrosis. They also reconcile previous conflicting results on the role of EMT[10-12] in this process, confirming the very limited contribution of a full EMT program that delivers transformed epithelial cells to the interstitium[13]. Importantly, the partial EMT undergone by renal epithelial cells and the persistence of the damaged tubules explains the high degree of cell plasticity that we observed *in vivo*, as we show that Snail1 inactivation in a epithelial specific Snail1-induced fibrosis model leads to the recovery of renal morphology and function. Furthermore, we also show that inhibition of Snail1 once fibrosis has been established can also ameliorate the disease. In relation to this, it is worth noting that Snail1 protects from cell death and decreases proliferation[30], suggesting that Snail1 reactivation in tubular cells would make cells survive and stay in the tubules although in an undifferentiated state. Subsequent Snail1 inhibition can help in the resolution of fibrosis by promoting the reversion of the damaged tubule cells to an epithelial phenotype and an

increase in proliferation. During TGF-β-induced EMT in cancer cells the mutual antagonism between Snail1 and miR-34 (ref. 31,32) has been recently considered as a reversible switch, pointing to the possibility of reversion to the epithelial phenotype in cancer cells[32] and miR-34c has been shown to attenuate UUO-induced fibrosis[33]. In cases of very advanced human renal fibrosis, where there is evidence of tubular atrophy, reversibility may be compromised. Although further investigation to assess the maximum degree of reversibility and the appropriate timing for intervention is warranted, our data encourage the design of anti-EMT/anti-Snail1 therapeutic strategies for the treatment of renal fibrosis.

Our data also help to better distinguish type 2 EMT, previously ascribed to fibrosis and wound healing, from type 3 EMT[34], associated with cancer cell delamination from the primary tumor. We see a partial EMT occurring in type 2, where damaged adult epithelial cells remain confined in their tissue of origin, without engaging into the delamination and invasion programs. A full EMT in cancer (type 3) endows cells with the ability to invade adjacent territories and to intravasate into blood vessels to later populate distant organs[25].

With regard to the link between fibrosis and inflammation we find that it also relies on the reactivation and, particularly, the maintenance of Snail1 expression in epithelial cells. UUO induces the activation of TGF- β and NF-κB signaling pathways, key for fibrogenesis and inflammation, respectively, and crucial drivers of CKD and other fibrotic processes[35,36]. The initial inflammatory response after UUO leads to TNF-α production, which induces the activation of NF-κB[34]. In addition to inflammation, NF-κB induces *Snai1* transcription and the

stabilization of the Snail1 protein[37]. TGF-β is first secreted to control the inflammatory response, but in the context of chronic injury as in fibrosis, it becomes fibrogenic and the most potent Snail inducer[4]. Thus, both signaling pathways converge on the activation of Snail1 and Snail1 activation and maintenance of its expression are required for the progression of fibrogenesis and for sustained inflammation (**Supplementary Fig. 10**). Thus, Snail1 establishes positive feedback loops reinforcing both the fibrogenic and inflammatory responses. As such, although we have not directly targeted TGF-β, we show that Snail1 is required for the maintenance of *Tgfb1* expression and signaling. Compatible with the establishment of feedback loops, we show that Snail1 mediates the induction of inflammatory cytokines and of TGF-β signaling as observed in cancer cells[19,22,23,36]. Interestingly, the inflammatory microenvironment in fibrosis appears to be similar to that in tumors. Altogether, this explains why in the absence of Snail1 reactivation in tubular cells, as in our SFKC model, both fibrogenesis and inflammation are highly attenuated, indicating that the partial EMT activated by Snail1 in renal epithelial cells is instrumental for the progression of renal disease.

Following the previous observations, Snail1 should behave as a promising therapeutic target. We find that after UUO, Snail1 inhibition by systemic injection of antisense oligonucleotides very significantly ameliorates fibrosis. Inhibiting EMT/inflammation by dowregulation of either TGF-β[38,39] or NF-κB[40,41] signaling pathways have provided hope for anti-fibrotic treatments, but the pleiotropic roles of both pathways, particularly the associated beneficial effects, limit the potential use of their inhibitors in systemic administration protocols[42,43]. Given that Snail1 is maintained almost silently in healthy adult

tissues[5], its inhibition should not cause undesirable side effects. Our data also provide a window of opportunity for the EMT inhibitors being developed for anti-metastatic therapies and recently challenged by the demonstration that cancer cells need to revert to the epithelial phenotype for successful metastatic colonization[44,45]. As such, inhibiting EMT in cancer patients may be counterproductive[25]. By contrast, the mesenchymal phenotype is the end stage in organ fibrosis and the reversion to the epithelial state should be fully beneficial. We propose that Snail1 is located at the center of a "core" pathway in fibrosis, defining "core" as a pathway which targeting is sufficient to limit the progression of the disease[42]. In summary, inhibiting EMT and Snail1 in particular can be regarded as a safe strategy to ameliorate fibrosis, especially in fibrotic processes where inflammation plays an important role in the progression of the disease.

ACKNOWLEDGMENTS

We thank members of Angela Nieto's lab for helpful discussions and comments along the years. We also thank Santiago Canals for his advice on statistical analysis, Christian Villena and Stuart Ingham for the design of Supplementary Figure 10. We are very grateful to Peter Igarashi (University of Texas Southwestern) for providing the Ksp1.3-Cre mice. This work was supported by grants from the Spanish Ministry of Economy and Competitiveness (BFU2008-01042 and CONSOLIDER-INGENIO 2010 CSD2007-00023 and CDS2007-00017), the Generalitat Valenciana (Prometeo 2008/049 and PROMETEOII/2013/002) and the European Research Council (ERC AdG 322694) to M.A.N. The Instituto de Neurociencias is a Centre of Excellence

Severo Ochoa. M.T.G. was recipient of a contract from the JAE-doc Program (CSIC-European Social Fund).

AUTHOR CONTRIBUTIONS

M.T.G. and B.S.-L. performed the majority of experiments, analyzed the data and contributed to writing the manuscript, C.L.-B. was instrumental in the surgery and histological and expression studies. C.A.F. and A.B. started the project, G.R. and S.J.W. provided the Snail1^{loxp} mice before publication, J.M.L.-N and M.A. quantified Sirius Red staining and J.M.L.-N. helped in the interpretation of data. M.A.N. conceived the project, interpreted the data and wrote the manuscript.

COMPETING FINANCIAL INTEREST

The authors declare no competing financial interests.

References

1. Liu, Y. Cellular and molecular mechanisms of renal fibrosis. *Nat. Rev. Nephrol.* **7**, 684-696 (2011).
2. National Kidney and Urologic Diseases Information Clearing House. Kidney Disease Statistics for the United States. No 12-3895 (2012).
3. Dressler, G. Tubulogenesis in the developing mammalian kidney. *Trends Cell Biol.* **12**, 390-395 (2002).
4. Thiery, J.P., Acloque, H., Huang, R.Y. & Nieto, M.A. Epithelial-mesenchymal transitions in development and disease. *Cell* **139**, 871-890 (2009).

5. Boutet, A.*, et al.* Snail activation disrupts tissue homeostasis and induces fibrosis in the adult kidney. *EMBO J.* **25**, 5603-5613 (2006).

6. Sato, M., Muragaki, Y., Saika, S., Roberts, A.B. & Ooshima, A. Targeted disruption of TGF-beta1/Smad3 signaling protects against renal tubulointerstitial fibrosis induced by unilateral ureteral obstruction. *J. Clin. Invest.* **112**, 1486-1494 (2003).

7. Lange-Sperandio, B.*, et al.* Leukocytes induce epithelial to mesenchymal transition after unilateral ureteral obstruction in neonatal mice. *Am. J. Pathol.* **171**, 861-871 (2007).

8. Grande, M.T.*, et al.* Deletion of H-Ras decreases renal fibrosis and myofibroblast activation following ureteral obstruction in mice. *Kidney Int.* **77**, 509-518 (2010).

9. Chevalier, R.L., Forbes, M.S. & Thornhill, B.A. Ureteral obstruction as a model of renal interstitial fibrosis and obstructive nephropathy. *Kidney Int.* **75**, 1145-1152 (2009).

10. Iwano, M.*, et al.* Evidence that fibroblasts derive from epithelium during tissue fibrosis. *J. Clin. Invest.* **110**, 341-350 (2002).

11. Humphreys, B.D.*, et al.* Fate tracing reveals the pericyte and not epithelial origin of myofibroblasts in kidney fibrosis. *Am. J. Pathol.* **176**, 85-97 (2010).

12. Li, L., Zepeda-Orozco, D., Black, R. & Lin, F. Autophagy is a component of epithelial cell fate in obstructive uropathy. *Am. J. Pathol.* **176**, 1767-1778 (2010).

13. LeBleu, V.S.*, et al.* Origin and function of myofibroblasts in kidney fibrosis. *Nat. Med.* **19**, 1047-1053 (2013).

14. Rowe, R.G.*, et al.* Mesenchymal cells reactivate Snail1 expression to drive three-dimensional invasion programs. *J. Cell Biol.* **184**, 399-408 (2009).

15. Shao, X., Somlo, S. & Igarashi, P. Epithelial-specific Cre/lox recombination in the developing kidney and genitourinary tract. *J. Am. Soc. Nephrol.* **13**, 1837-1846 (2002).

16. Franci *et al*. Expression of Snail in tumor-stroma interface. *Oncogene* **25**, 5134-5144 (2006).

17. Costa, M.Z., Bacchi, C.E., & Franco, M. Histogenesis of the acquired cystic kidney disease: an immunohistochemical study. *Appl. Immunohistochem. Mol. Morphol.* **14**, 348-352 (2006).

18. Borges, F.T.*, et al.* TGF-beta1-containing exosomes from injured epithelial cells activate fibroblasts to initiate tissue regenerative responses and fibrosis. *J. Am. Soc. Nephrol.* **24**, 385-392 (2013).

19. Dhasarathy, A., Phadke, D., Mav, D., Shah, R.R. & Wade, P.A. The transcription factors Snail and Slug activate the transforming growth factor-beta signaling pathway in breast cancer. *PLoS One* **6** (10):e26514 (2011).

20. Grande, M.T., Pérez-Barriocanal, F., López-Novoa, J.M. Role of inflammation in tubulo-interstitial damage associated to obstructive nephropathy. *J. Inflamm.* (Lond). **7**, 19 (2010).

21. Biswas, S.K. & Mantovani, A. Macrophage plasticity and interaction with lymphocyte subsets: cancer as a paradigm. *Nat. Immunol.* **11**, 889-896.

22. Lyons, J.G. *et al.* Snail up-regulates proinflammatory mediators and inhibits differentiation in oral keratinocytes. *Cancer Res.* **68**, 4525-4530

(2008).

23. Hsu D.S., *et al.* Acetylation of Snail modulates the cytokinome of cancer cells to enhance the recruitment of macrophages. *Cancer Cell* **26**, 534-548 (2014).

24. Yang, H.-C., Zuo, Y. & Fogo, A.B. Models of chronic disease. *Drug Discov. Today Dis. Models,* **7**, 13-19 (2010).

25. Nieto, M.A. Epithelial plasticity: a common theme in embryonic and cancer cells. *Science* **342**, 1234850 (2013).

26. Kriz, W., Kaissling, B. & Le Hir, M. Epithelial-mesenchymal transition (EMT) in kidney fibrosis: fact or fantasy? *J. Clin. Invest.* **121**, 468-474 (2011).

27. Fragiadaki, M. & Mason, R.M. Epithelial-mesenchymal transition in renal fibrosis - evidence for and against. *Int. J. Exp. Pathol.* **92**, 143-150 (2011).

28. Zeisberg, M. & Neilson, E.G. Mechanisms of tubulointerstitial fibrosis. *J. Am. Soc. Nephrol.* **21**, 1819-1834 (2010).

29 . Meng, X.M., Nikolic-Paterson, D.J. & Lan, H.Y. Inflammatory processes in renal fibrosis. *Nat. Rev. Nephrol.* (2014).

30. Vega S, Morales AV, Ocaña OH, Valdés F, Fabregat I, Nieto MA. Snail blocks the cell cycle and confers resistance to cell death. *Genes Dev*. **10**, 1131-43 (2004).

31. Kim, N.H.*, et al.* A p53/miRNA-34 axis regulates Snail1-dependent cancer cell epithelial-mesenchymal transition. *J. Cell Biol.* **195**, 417-433 (2011).

32. Tian, X.J., Zhang, H. & Xing, J. Coupled reversible and irreversible bistable switches underlying TGFbeta-induced epithelial to mesenchymal transition. *Biophys. J.* **105**, 1079-1089 (2013).

33. Morizane, R.*, et al.* miR-34c attenuates epithelial-mesenchymal transition and kidney fibrosis with ureteral obstruction. *Sci. Rep.* **4**, 4578 (2014).

34. Kalluri, R. & Weinberg, R.A. The basics of epithelial-mesenchymal transition. *J. Clin. Invest.* **119**, 1420-1428 (2009).

35. Liu, Y. Renal fibrosis: new insights into the pathogenesis and therapeutics. *Kidney Int.***69**, 213-217 (2006).

36. Lopez-Novoa, J.M. & Nieto, M.A. Inflammation and EMT: an alliance towards organ fibrosis and cancer progression. *EMBO Mol. Med.* **1**, 303-314 (2009).

37. Wu, Y.*, et al.* Stabilization of snail by NF-kappaB is required for inflammation-induced cell migration and invasion. *Cancer Cell* **15**, 416-428 (2009).

38. Rosenbloom, J., Castro, S.V. & Jimenez, S.A. Narrative review: fibrotic diseases: cellular and molecular mechanisms and novel therapies. *Annals Int. Med.* **152**, 159-166 (2010).

39. Zeisberg, M.*, et al.* BMP-7 counteracts TGF-beta1-induced epithelial-to-mesenchymal transition and reverses chronic renal injury. *Nat. Med.* **9**, 964-968 (2003).

40. Esteban, V.*, et al.* Angiotensin II, via AT1 and AT2 receptors and NF-kappaB pathway, regulates the inflammatory response in unilateral ureteral obstruction. *J. Am. Soc. Nephrol.* **15**, 1514-1529 (2004).

41. Miyajima, A.*, et al.* Novel nuclear factor kappa B activation inhibitor prevents inflammatory injury in unilateral ureteral obstruction. *J. Urol.* **169**, 1559-1563 (2003).

42. Mehal, W.Z., Iredale, J. & Friedman, S.L. Scraping fibrosis: expressway to the core of fibrosis. *Nat. Med.* **17**, 552-553 (2011).

43. Luedde, T. & Schwabe, R.F. NF-kappaB in the liver--linking injury, fibrosis and hepatocellular carcinoma. *Nat. Rev. Gastroenterol. Hepatol.* **8**, 108-118 (2011).

44. Tsai, J.H., Donaher, J.L., Murphy, D.A., Chau, S. & Yang, J. Spatiotemporal regulation of epithelial-mesenchymal transition is essential for squamous cell carcinoma metastasis. *Cancer Cell* **22**, 725-736 (2012).

45. Ocana, O.H.*, et al.* Metastatic colonization requires the repression of the epithelial-mesenchymal transition inducer Prrx1. *Cancer Cell* **22**, 709-724 (2012).

FIGURE LEGENDS

Figure 1 Snail reactivation is required for the development of UUO-induced fibrosis. (**a**) Scheme of the experimental approach. UUO was conducted in wild type (WT) or Ksp1.3-Cre;Snai1$^{fl/fl}$ (SFKC) mice, which were sacrificed 7 or 15 days after obstruction. (**b**) *Snai1* mRNA levels determined by qRT-PCR in obstructed (L) and in contralateral non-obstructed kidneys (NL) from WT and SFKC mice 7 or 15 days after UUO. (**c**) Representative images of kidney sections stained by *in situ* hybridization for *Snai1* from sham-operated (control) and obstructed kidneys (UUO) of WT and SFKC mice 15 days after surgery. (**d**)

Representative images of similar sections showing hematoxylin-eosin (H&E) and Sirius red stainings, and in (**e**) alpha smooth muscle actin (α-SMA) or vimentin immunohistochemistry. Tissue sections in c-e are representative of 8 independent samples from 5 mice per group (**f**) *Snai2*, *Cadh1*, *Cadh16*, *Vim*, *Acta2* and *Col1a1* mRNA levels detected by qRT-PCR. (**g**) Sirius red staining quantification as a measure of overall cortical fibrosis. Data are shown for obstructed kidneys from WT (n = 4) and SFKC (n = 3) mice relative to kidneys from sham-operated mice. ****P< 0.0001; Mann-Whitney test; Error bars show means ± SEM. (**h**) *Tgfb1* mRNA levels in obstructed (L) and contralateral non-obstructed (NL) kidneys from WT and SFKC mice. For all qRT-PCR experiments, data are normalized to levels in sham-operated mice and represent mean ± SEM for groups of 7 mice**.** **P < 0.01, ***P < 0.001, ****P < 0.0001; Two-way ANOVA followed by Tukey's multiple comparison test. Scale bars, 50 μm.

Figure 2 Renal epithelial cells undergo a partial EMT after UUO. **(a)** Ksp1.3-Cre;tdTomato$^{fl/fl}$ mice were subjected to UUO and kidneys were collected 15 days after surgery. Representative images (n = 20) of sections of kidneys from Ksp1.3-Cre;tdTomato$^{fl/fl}$ mice (KCT) 15 d after being subjected to UUO. Images are for obstructed (KCT+UUO) and contralateral non-obstructed kidneys (Control) from KCT mice stained for LTA (*Lotus tetragonolobus* agglutinin) +PNA (Peanut agglutinin) markers of proximal and distal tubules[17]), α-SMA and DAPI. tdTomato fluorescent protein expression was directly visualized. Asterisks indicate α-SMA expression in tubular cells that have lost lectin expression 15 days after UUO. (**b**) Number of dilated and total tubules in

kidneys from WT and SFKC mice 15 days after UUO. 10 different fields were counted in 12 mice per group. Data represent mean ± SEM. *$P < 0.05$, NS, non-significant; Mann-Whitney test. **(c)** Representative images (n = 5) of double Snail1 and α-SMA immunolabeling in sections from obstructed kidneys of WT mice sacrificed 15 days after surgery. Red asterisks indicate Snail1 positive nuclei. Green asterisks indicate double positive Snail1 and α-SMA tubular cells. dt, dilated tubule, g, glomerulus, t, tubule. (**d**) Representative images (n = 5) of lectin (LTA) and Snail1 immunofluorescence in sections from the same kidneys used in **b**. Scale bars, 50 μm.

Figure 3 Snail1 reactivation in renal epithelial cells is required for sustained inflammation in the injured kidney. The experimental design is the same as in **Fig. 1**. (**a**) Representative images (n = 5) of immunolabeling for phospho-NF-κB (pNF-κB); F4/80 (pan-macrophage marker) and CD163 (M2-macrophage marker) in obstructed (L) and contralateral control (NL) kidneys from WT and SFKC mice collected 15 days after surgery. Tissue sections are representative of 5 mice per group. (**b**) Cytokines levels detected in 15 days-obstructed SFKC kidneys relative to those in 15 days-obstructed WT lysates. Error bars represent mean ± SEM. (**c**) *Tnfa, Ccl2* and *Ccl5* mRNA levels determined by qRT-PCR in obstructed (L) and in contralateral non-obstructed kidneys (NL) from both WT and SFKC mice, 3, 7 or 15 days after UUO. (**d**) Representative images (n = 5) of kidney sections stained for H&E (top) and phospho-NFκB (pNF-κB) (bottom) from sham-operated (control) and obstructed kidneys (UUO) of WT and SFKC mice 3 days after surgery. Tissue sections are representative of 3 mice per group. (**e**) *Snai1* and *Tgfb1* mRNA levels in the kidneys shown in **d**. All qRT-

PCR data are normalized to sham-operated wild type levels and represent mean ± SEM for groups of 3 mice**.** ***P* < 0.5**,** ****P* < 0.1, ****P* < 0.01, *****P* < 0.0001; Two-way ANOVA followed by Tukey's Multiple comparison test. Scale bars, 50 μm.

Figure 4 Snail reactivation is required for the development of folic acid-induced fibrosis. Folic acid (FA) was administered to WT or SFKC mice, which were sacrificed 34 d after FA administration. (**a**) Representative images (*n* = 5) of H&E and Sirius red stainings and LTA, PNA, α-SMA, F4/80 and CD163 immunohistochemistry on sections from WT and SFKC mice treated with vehicle or folic acid (FA). Tissue sections are representative of 5 mice per group. (**b**) *Snai1, Col1a1, Cadh1, Cadh16*, *Vim, Acta2, Tgfb1, Tnfa, Ccl2 and Ccl5* mRNA levels determined by qRT-PCR in vehicle (Control) or FA treated WT and SFKC mice. Data are normalized to vehicle-treated WT levels and represent mean ± SEM for groups of 4 mice**.** ****P* < 0.01, *****P* < 0.001, ******P* < 0.0001; One-way ANOVA followed by Tukey's multiple comparison test. (**c**) Kidney lysates from WT or SFKC mice treated with FA were incubated with a cytokine array. Data represent the signals detected for specific cytokines in SFKC lysates relative to those in WT lysates. Error bars represent mean ± SEM. (**d**) Sirius red staining was quantified and represented relative to vehicle-treated mice in 3 mice per group. ******P* < 0.0001; Mann-Whitney test. Error bars show means ± SEM. Scale bars, 50 μm.

Figure 5 Snail1-induced fibrosis can be reversed *in vivo*. (**a**) Scheme of the experimental approach. Mice were treated with (1) vehicle (corn oil, –TAM); (2)

tamoxifen for 8 weeks (+TAM); (3) tamoxifen for 8 weeks followed by vehicle treatment for another 8 weeks (+TAM–TAM). (**b**) Anti-human estrogen receptor (hER) immunohistochemistry showing exogenous Snail1 protein expression and activation upon tamoxifen treatment. (**c**) Representative images (*n* = 6 samples from 6 mice per group) of H&E and Sirius Red staining, and alpha smooth muscle actin (α-SMA), vimentin, phospho-NF-κB (pNF-κB), F4/80 and CD163 immunohistochemistry from kidney sections from mice in **a**. (**d**) mRNA levels detected by qRT-PCR in kidneys from Snail1-ERT2 mice showing *Snai2*, *Vim*, *Tgfb1 Cadh1* and *Cadh16* abundance upon Snail1 activation (2:+TAM) and deactivation after 8 weeks of tamoxifen removal (3:+TAM–TAM). Data are normalized to vehicle treated kidney levels (1; –TAM) and represent mean ± SEM for groups of 4 mice**.** **P*< 0.05, ***P* < 0.01, ****P* < 0.001, *****P* < 0.0001; One-way ANOVA followed by Tukey's multiple comparison test. (**e**) Morphometric analysis of cortical interstitial fibrosis by quantification of Sirius Red staining. Data are shown relative to vehicle treated controls (4 mice per group). ***P* < 0.01, ****P* < 0.001, **** *P*< 0.0001; One-way ANOVA followed by Tukey's multiple comparison test. Error bars show means ± SEM. Scale bars, 50 μm

Figure 6 Snail1 inactivation reverts UUO-induced fibrosis in mice. (**a**) Scheme of the experimental approach. Seven days after UUO, mice were injected with vivo-morpholino control (Control-MO) or Snail1-MOs (Snail1-MO1 or Snail-MO2; **Supplementary Fig. 11**) every other day. Shown are the results obtained in mouse #5, representative of those in which the VIVO morpholino efficiently prevented Snail1 normal splicing. (**b**) Representative images (*n* = 5) of H&E and

Sirius Red staining and immunohistochemistry of mesenchymal (vimentin and alpha smooth muscle actin (α-SMA)) and inflammatory response markers (F4/80 and phospho-NFkB (pNFκB)) in kidney sections from mice in **a**. (**c**) *Snai1, Snai2, Vim, Tgfb1, Cadh1 and Cadh16* mRNA levels detected by qRT-PCR in obstructed kidneys from WT mice treated with Snail1-MO. Data are normalized to contralateral non-obstructed kidney levels (NL) and represent mean ± SEM for triplicates of data from a representative mouse in which Snail1-MO efficiently induced exon-skipping and *Snai1* downregulation**.** **P* < 0.05, ***P* < 0.01, ****P* < 0.001, *****P* < 0.0001; Two-way ANOVA followed by Tukey's multiple comparison test. (d) Sirius red quantification in the renal cortex of mice injected with Control-MO (average values from 4 mice) or Snail1-MO (mouse #5). *****P*< 0.0001; Mann-Whitney test. Error bars show means ± SEM. Scale bars, 50 μm.

ONLINE METHODS

Mice. All animal procedures were conducted in strict compliance with the European Community Council Directive (89/609/EEC) and the Spanish legislation. Ethical protocols were approved by the CSIC Ethical Committee and the Animal Welfare Committee of the Institute of Neurosciences. Animals for experiments were selected by genotype, no randomization or blinding was performed. Animals were housed under SPF conditions at the RMG animal House (ES-119-002001 SEARMG). Work with GMO was under the A1ES/13/1-25 license. To specifically inactivate Snail1 in renal epithelial cells, we generated a mouse line with kidney-specific inactivation of Snail1 by crossing females from the Snail1-floxed line ($Snai1^{fl/fl}$)[14] with the Ksp-Cre transgenic

strain obtained from Peter Igarashi´s lab[15]. R26R mice (Gtrosa26tm1Sor) were obtained from Jackson Laboratories. To examine the efficiency of recombination, heterozygous female Snail1 floxed mice (Snail1$^{fl/+}$) were crossed with heterozygous male mice that express Ksp1.3-Cre transgene. From the filial (F) 1 progeny, mice (male or female), litters with heterozygous deletion of *Snai1* gene that harbored the Ksp1.3/Cre transgene (*Snail1$^{fl/+}$; Ksp1.3-Cre*) were selected and they were further crossed with the opposite sex of Snail1 floxed mice (Snai1$^{fl/+}$) to obtain mice expressing complete deletion of Snail1 in the F2 progeny (Snai1$^{fl/fl}$;Ksp1.3-Cre), referred to as SFKC. Compared to control (*Snail1$^{fl/fl}$*) littermates, SFKC mice are viable, display no overt defects, and survive to 6 months and beyond with no ill effects. The generation of the tamoxifen-inducible Snail1 transgenic mouse has been described previously[5] where the transgenic Snail1-ERT2 protein was specifically expressed in renal epithelial cells (**Supplementary Fig. 7**). In this model, constitutively expressed exogenous Snail1 protein only becomes active on nuclear translocation. For tamoxifen inductions, the tamoxifen was dissolved in corn oil 30 mg/ml and mice (8 weeks-old) were intraperitoneally injected with 200 mg of tamoxifen per gram of body weight or a similar volume of corn oil every 3 days for 8 or 16 weeks. For lineage tracing experiments Ksp1.3-Cre mice were crossed with Rosa-LSL-TdTomato mice (Stock number: 007905 from Jackson Laboratories). In these mice, fluorescent tdTomato is expressed following Cre-mediated recombination. Animals were killed by cervical dislocation and their kidneys processed for mRNA extraction, ISH, immunohistochemistry or cytokines extraction. 8 weeks-old male mice were used for the experiments.

UUO model. Male mice (8 weeks-old) were anesthetized with an intraperitoneal injection of ketamine (100 mg/kg) and xylazine (10 mg/kg). The abdomen was opened, and the left ureter was ligated with 5-0 silk. The abdomen was then closed with running sutures and the skin was closed with interrupted sutures. After surgery, the mice were maintained in a temperature-controlled room with a 12 hours light/dark cycle, and were reared on standard chow and water ad libitum. Unilateral ureteral obstruction (UUO) was maintained for 3, 7 or 15 days.

In situ **hybridization.** In situ hybridization was performed as previously described[3]. Briefly, mouse kidneys were fixed overnight in 4% PFA in PBS and processed directly for paraffin embedding. 12 µm sections were de-paraffinized and rehydrated, treated with proteinase K and fixed with 4% paraformaldehyde. Digoxigenin-labeled RNA probes were detected by alkaline-phosphatase-coupled anti-digoxigenin antibody (Roche Diagnostics, Mannheim, Germany) and NBT/BCIP was used as a chromogenic substrate to detect the digoxigenin-labeled probes (Boehringer, Mannheim, Germany). Sections were mounted in 50% glycerol in PBS and slices were photographed with a Leica DMR microscope under Nomarski optics.

Histological analysis. Kidney tissues were fixed in 4% PFA in PBS for 24 hours and embedded in paraffin. 8-µm sections were cut using a paraffin microtome with stainless steel knives. The sections were mounted on glass slides, deparaffinized with xylene, dehydrated through graded series of ethanol, and stained with hematoxylin-eosin. To evaluate collagen deposition, sections

were stained with Sirius Red (saturated aqueous solution of picric acid containing 0.1% Direct Red 80) (Sigma-Aldrich, St Louis, MO).

Immunohistochemical studies. Paraffin sections were deparaffinized and hydrated in graded ethanol series before staining with the peroxidase–antiperoxidase method. Antigens were retrieved by boiling for 20 min in 10mM citric acid solution (pH=6) or 10 mM Tris- 1 mM EDTA (pH=9). Endogenous peroxidase was blocked by incubation in 4% hydrogen peroxide. The sections were incubated overnight at 4ºC with the following primary antibodies: Biotinylated *Lotus Tetragonolobus* agglutinin, LTA (B-1325, Vector Laboratories, Burlingame, CA); Biotinylated Peanut agglutinin, PNA (B-1075, Vector Laboratories, Burlingame, CA); alpha-smooth muscle actin, α-SMA (Sigma-Aldrich, St Louis, MO); Vimentin (sc-7557, Santa Cruz Biotechnology, Santa Cruz, CA); Snail1 (Ab1773; Abcam PLC, Cambridge, MA); Phospho-NF-κB p65 (Ser276) (3037S, Cell Signaling Technology, Inc., Danvers, MA); Phospho-Smad2 (Ser465/467) (3101S, Cell Signaling Technology, Inc., Danvers, MA); F4/80 (MCA497GA, Serotec, Oxford,UK); Estrogen receptor alpha, ERα (sc-543, Santa Cruz Biotechnology, Santa Cruz, CA); CD163 (sc-18796 Santa Cruz Biotechnology, Santa Cruz, CA). The sections were incubated with the corresponding biotinylated secondary antibodies, and sequentially incubated in ABC-Peroxidase Solution (Thermo Scientific, Rockford, IL) and 3,3'-Diaminobenzidine (DAB) (Sigma-Aldrich, St Louis, MO) was used as chromogen. Sections were lightly counterstained with hematoxylin and were dehydrated and coverslipped.

X-Gal Staining. Kidneys were fixed in 4% paraformaldehyde in PBS for 2 hours on ice and stained for β-galactosidase activity by incubation in PBS containing 2 mM $MgCl_2$, 5 mM K4Fe(CN)6, 5 mM K3Fe(CN)6, and 0.4 mg/ml X-gal overnight at 37°C. After staining, the kidneys were washed in PBS and further fixed in 4% paraformaldehyde in PBS at 4°C. Kidneys were embedded in paraffin and 5 μm sections were cut, mounted and photographed with a Leica DMR microscope. In some experiments tissue sections were sequentially stained with antibodies or lectins as described above.

Quantitative RT-PCR (qRT-PCR). Total RNA was extracted using the Illustra RNAspin Mini RNA isolation kit (GE Healthcare, Little Chalfont, UK). 1μg of RNA was reverse transcribed using random hexamer primers according to the manufacturer's instructions (SuperScript II, Invitrogen). qRT-PCR was carried out on an ABI PRISM 7000 sequence detection system using the SYBR Green method (Applied Biosystems). RNA expression was calculated using the comparative Ct method normalized to Eif3. Data were expressed relative to a calibrator using the 2-($\Delta\Delta$Ct) ± s formula.

Immunofluorescence. Paraformaldehyde-fixed kidneys were immersed in 30% sucrose overnight and embedded in OCT for freezing. Slides were washed with PBS and blocked in PBS–Tween 0.1% + 1% BSA for 15 min. Sections were incubated at 4ºC overnight with the following primary antibodies: LTA (B-1325, Vector Laboratories, Burlingame, CA), PNA (B-1075, Vector Laboratories, Burlingame, CA); alpha-smooth muscle actin, α-SMA (Sigma-Aldrich, St Louis, MO) Snail (ab 1773; Abcam PLC, Cambridge, MA). Antibody detection was

performed with Alexa Fluor–conjugated secondary antibodies (Invitrogen). Slides were counterstained with DAPI. Samples were analyzed, and pictures were taken using a Leica DMR fluorescence or a Leica SP2 confocal scanning microscope (Leica Microsystems).

Cytokine array. A panel of cytokines in kidney lysates were detected using the mouse cytokine Array Kit, Panel A (#ARY006, R&D Systems, Minneapolis, MN, USA), following the manufacturer's instructions.

Folic acid-induced fibrosis model. Male mice (8 weeks-old) were intraperitoneally injected with a single dose of vehicle (300 mM $NaHCO_3$) or folic acid (250 μg/g BW). Kidneys were collected 34 days after injection.

Renal function. Twenty-four-hour urine was collected from tamoxifen-inducible Snail1 transgenic mice, at baseline and after 8 or 16 weeks of tamoxifen or vehicle administration. Animals were housed in a metabolic cage for collection of urine to determine creatinine concentration and urine volume. Blood was obtained from the saphenous vein. Creatinine concentration in plasma and urine was measured using the Reflotron® Creatinine kit (Roche Diagnostics, Mannheim, Germany) following the manufacturer's instructions. Creatinine clearance, an estimate of glomerular filtration rate, was calculated from plasma and urine creatinine concentration and urinary flow using standard formulae.

Morpholino oligomer and in vivo treatment. The oligonucleotides sequences 5′-TGAACTCTGCGGGAAGAGAAGAGAC-3′ VM1 against the boundary

sequences of the intron 1 and exon 2 and 5´-GCTATGCACACTCACTCACCAGTGT-3´ VM2 against the boundary sequences of the exon and intron 2 of Snail1 gene were synthesized as Morpholinos by (Gene Tools). Vivo-Morpholinos were made by conjugation of an unmodified Morpholino with a synthetic scaffold featuring eight guanidinium head groups. A control antisense that targets a human β-globin intron mutation 5′-CCTCTTACCTCATTACAATTTATA-3′ was used as vivo-morpholino standard control, VMC. C57/Bl6J male mice aged 8 weeks were subjected to UUO and 7 days after obstruction they were injected every other day until day 15. A solution of containing vivo-Morpholinos in saline (100 µL; 6mg MO/kg) was injected in the tail vein of the corresponding mice.

Quantification.

Sirius Red. Renal sections 5 µm thick were stained with Sirius red to evaluate the area occupied by collagen fibrils. From each kidney, a total of 10 interstitial random cortical fields were captured at 20-fold magnification using a green optical filter (IF 550) and a high-resolution video camera (SONY CCD-iris) connected to a light microscope (LEITZ Laborlux S). The area occupied by collagen was measured using a computerized image analysis system (Fibrosis HRR, Master Diagnostica) as previously described[46]. The values obtained for tubulointerstitial fibrotic tissue were expressed in square micrometers and are represented in the figures relative to control kidneys.

Immunofluorescence. For quantification of fluorescence images 20 random fields were visualized and the number of tdTomato or SMA positive cells was counted. Fields were observed at 400x magnification in a Leica DMR

fluorescence microscope. In addition, five random fields were photographed with a Leica SP2 confocal scanning microscope (Leica Microsystems) and cells counted.

Data analysis. Statistical analysis was performed using the GraphPad Prism software package. Results were expressed as mean ± SEM (standard error of mean). Data was normally distributed and the variance between groups was not significantly different. Differences among different groups were tested by One-Way ANOVA or Two-Way ANOVA followed up by Tukey's test as appropriate. Differences between two groups were tested using Mann-Whitney test. Sample size was selected following the recommendations from the "Organo Evaluador de Proyectos" (Committee for pre-evaluation of projects, University Miguel Hernandez) to calculate the size of the cohorts and following the requirements for the principles of the "3Rs" (reduction, refinement and replacement). No randomization, blinding or exclusion criteria were performed.

SUPPLEMENTARY REFERENCES

46. Rodríguez-López, A., Flores, O., Arévalo, M. & López-Novoa, J.M. Glomerular cell proliferation and apoptosis in the early phase of renal damage in uninephrectomized spontaneously hypertensive rats. *Kidney Int*. 54: S36–S40 (1998).

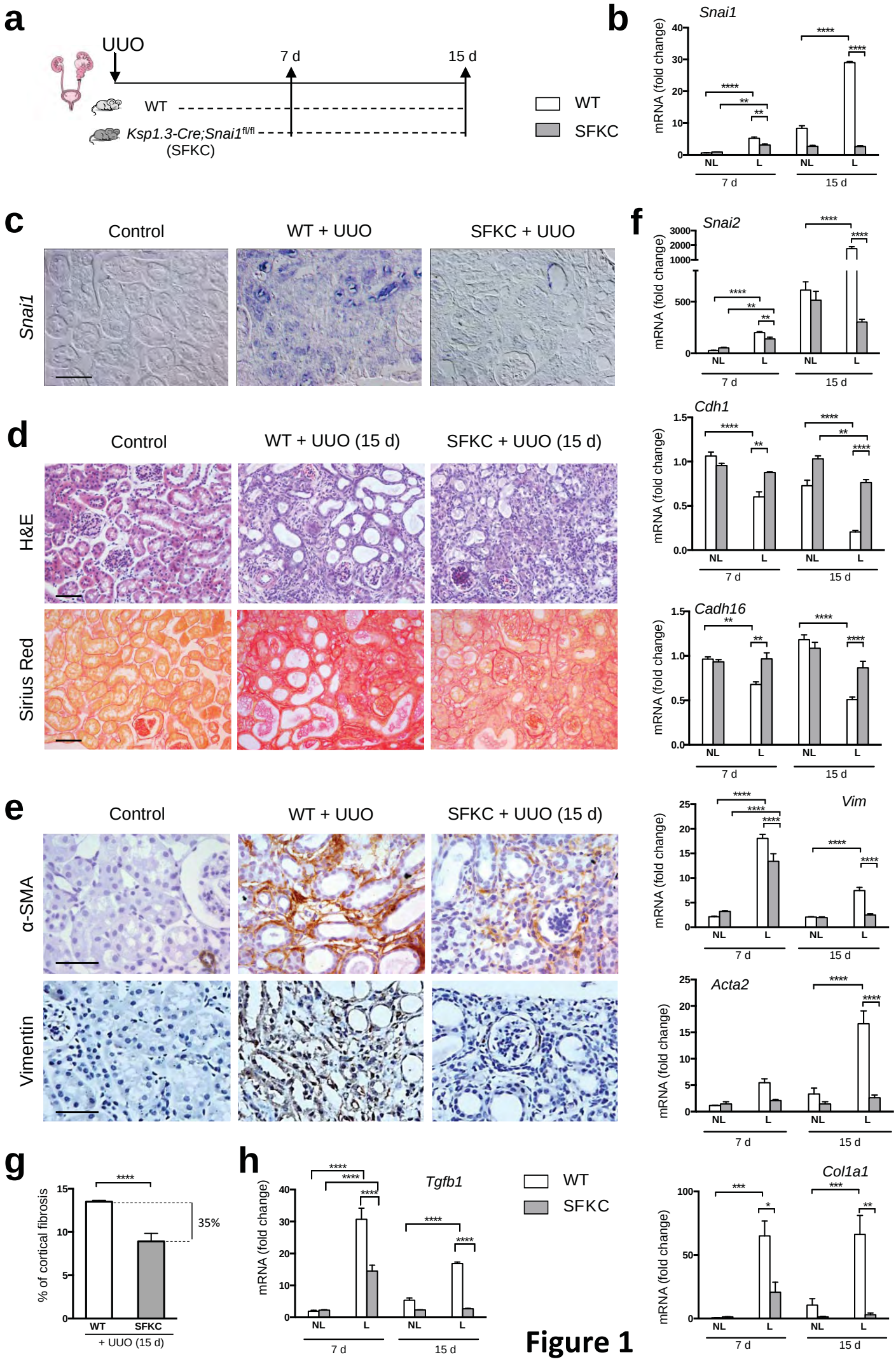
a
UUO
7 d
15 d
WT
Ksp1.3-Cre;Snai1fl/fl
(SFKC)
WT
SFKC
b
Snai1
mRNA (fold change)
NL
L
7 d
15 d
c
Control
WT + UUO
SFKC + UUO
Snai1
d
Control
WT + UUO (15 d)
SFKC + UUO (15 d)
H&E
Sirius Red
e
Control
WT + UUO
SFKC + UUO (15 d)
α-SMA
Vimentin
f
Snai2
Cdh1
Cadh16
Vim
Acta2
Col1a1
g
% of cortical fibrosis
35%
WT
SFKC
+ UUO (15 d)
h
Tgfb1
WT
SFKC

Figure 1

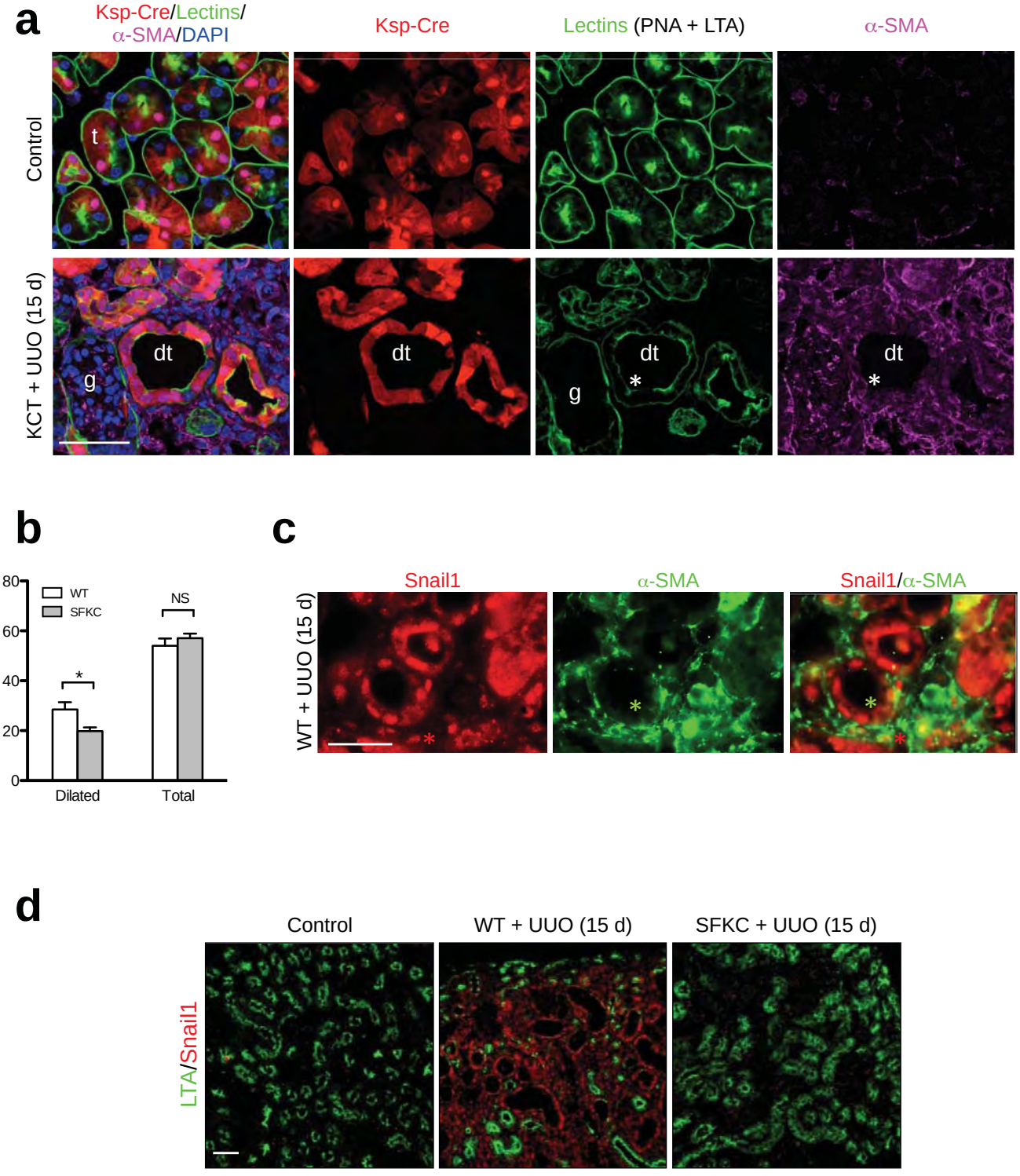
a
Ksp-Cre/Lectins/
α-SMA/DAPI
Ksp-Cre
Lectins (PNA + LTA)
α-SMA
Control
KCT + UUO (15 d)
t
dt
g
*
b
No. of tubular cross sections
WT
SFKC
NS
*
Dilated
Total
c
Snail1
α-SMA
Snail1/α-SMA
WT + UUO (15 d)
d
Control
WT + UUO (15 d)
SFKC + UUO (15 d)
LTA/Snail1

Figure 2

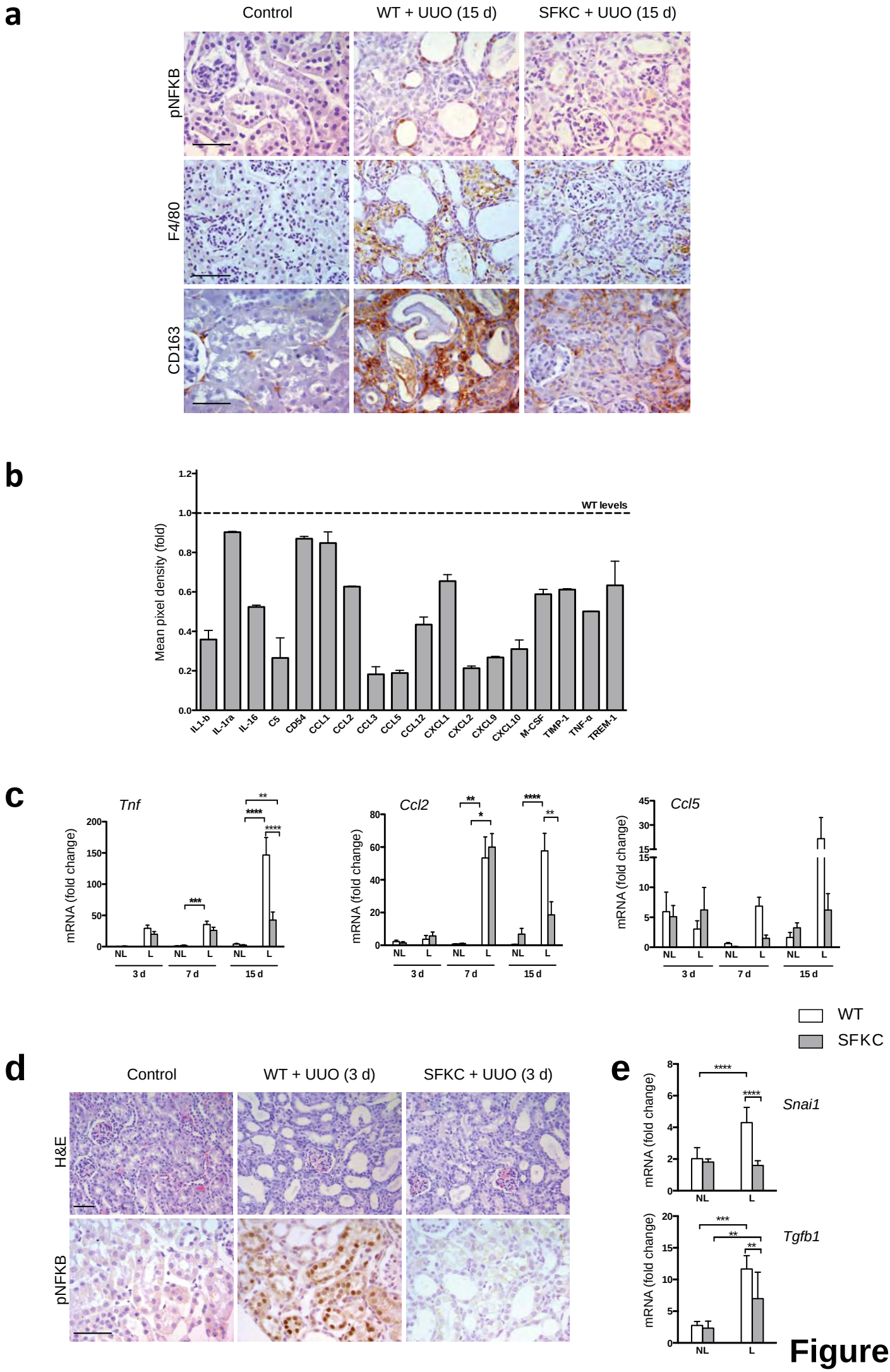
a
Control
WT + UUO (15 d)
SFKC + UUO (15 d)
pNFKB
F4/80
CD163
b
Mean pixel density (fold)
WT levels
IL1-b
IL-1ra
IL-16
C5
CD54
CCL1
CCL2
CCL3
CCL5
CCL12
CXCL1
CXCL2
CXCL9
CXCL10
M-CSF
TIMP-1
TNF-α
TREM-1
c
Tnf
Ccl2
Ccl5
mRNA (fold change)
NL
L
3 d
7 d
15 d
WT
SFKC
d
Control
WT + UUO (3 d)
SFKC + UUO (3 d)
H&E
pNFKB
e
Snai1
Tgfb1
mRNA (fold change)

Figure 3

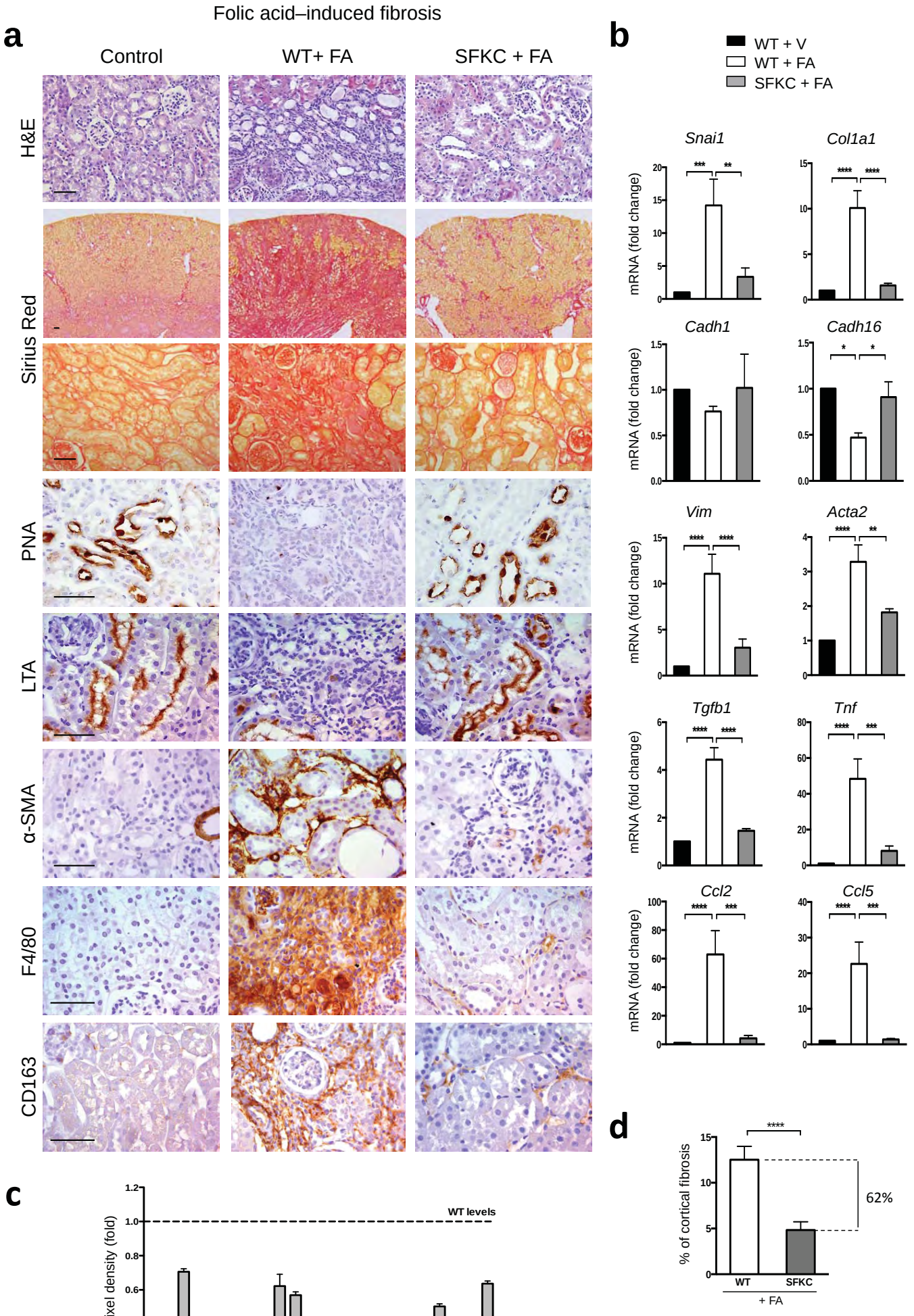
a
Folic acid–induced fibrosis
Control
WT+ FA
SFKC + FA
H&E
Sirius Red
PNA
LTA
α-SMA
F4/80
CD163
b
WT + V
WT + FA
SFKC + FA
Snai1
Col1a1
Cadh1
Cadh16
Vim
Acta2
Tgfb1
Tnf
Ccl2
Ccl5
mRNA (fold change)
c
WT levels
Mean pixel density (fold)
BLC
C5
CD54
IL1-ra
IL10
IL13
IL16
IL17
IL23
CCL1
CCL2
CCL3
CCL4
CCL5
CCL12
CXCL1
CXCL2
CXCL9
M-CSF
GM-CSF
TIMP-1
TNF-α
d
% of cortical fibrosis
62%
WT
SFKC
+ FA

Figure 4

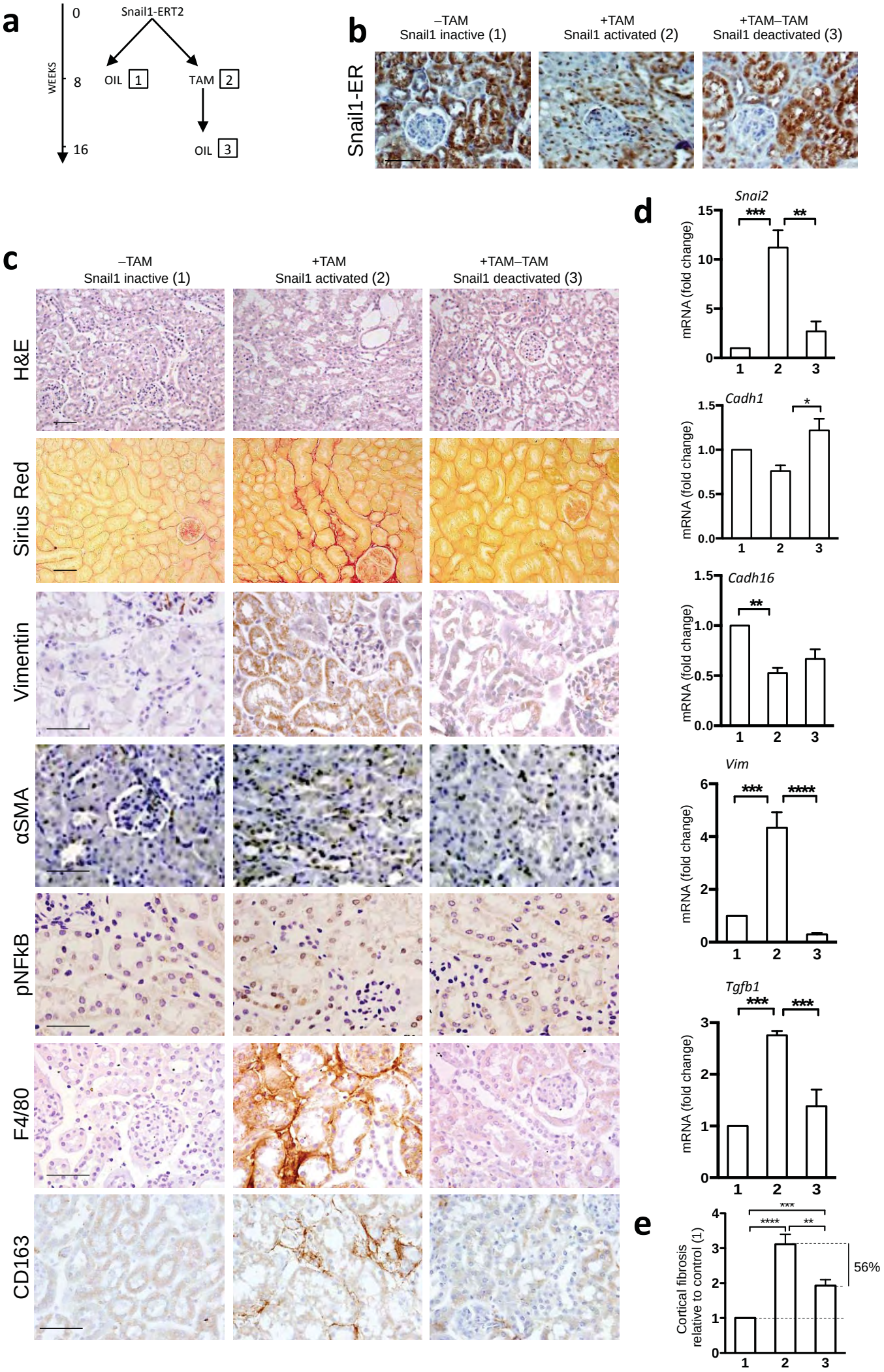
a
Snail1-ERT2
WEEKS
0
8
16
OIL 1
TAM 2
OIL 3
b
–TAM
Snail1 inactive (1)
+TAM
Snail1 activated (2)
+TAM–TAM
Snail1 deactivated (3)
Snail1-ER
c
–TAM
Snail1 inactive (1)
+TAM
Snail1 activated (2)
+TAM–TAM
Snail1 deactivated (3)
H&E
Sirius Red
Vimentin
αSMA
pNFkB
F4/80
CD163
d
Snai2
Cadh1
Cadh16
Vim
Tgfb1
mRNA (fold change)
e
Cortical fibrosis
relative to control (1)
56%

Figure 5

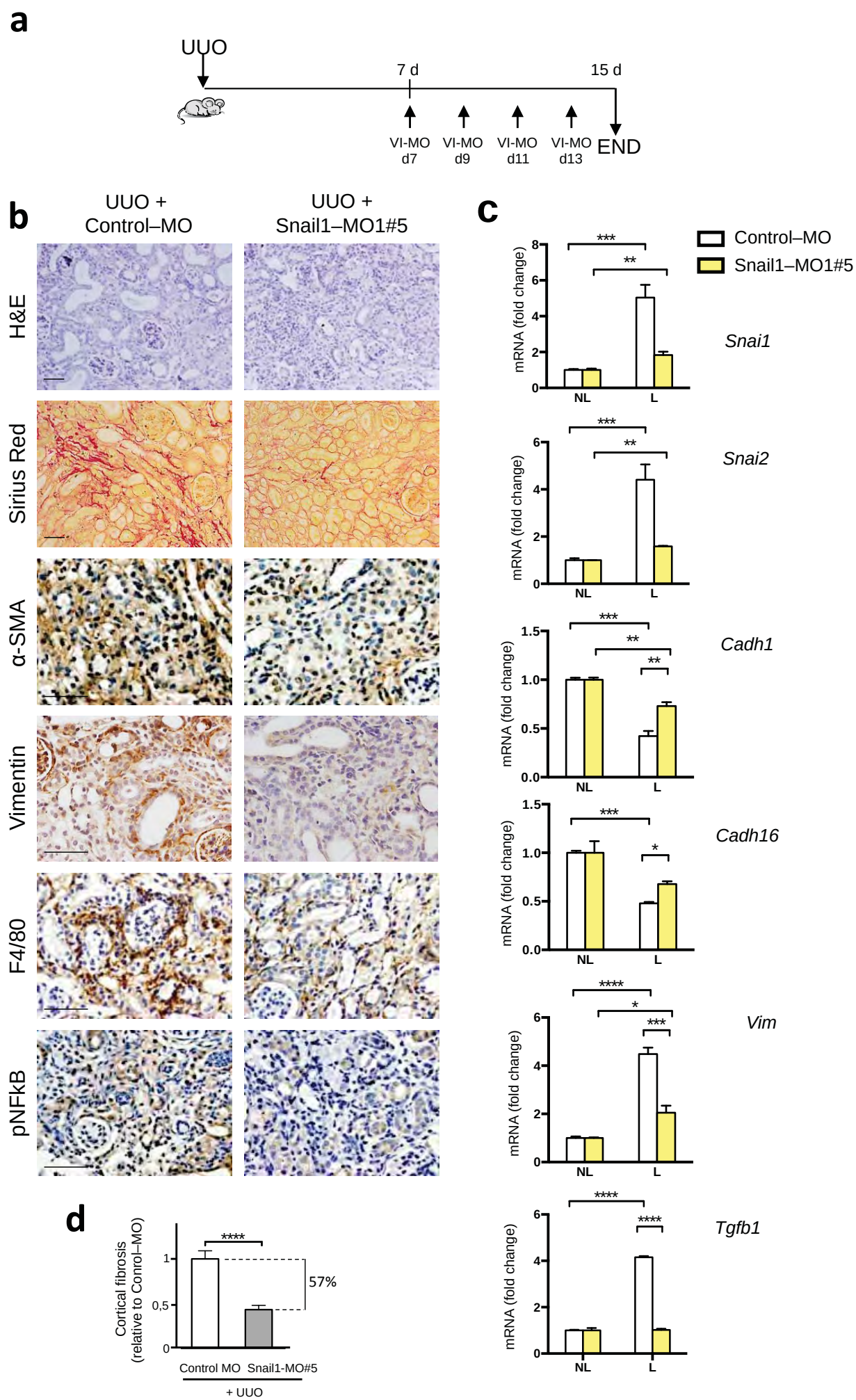
a
UUO
7 d
15 d
VI-MO d7
VI-MO d9
VI-MO d11
VI-MO d13
END
b
UUO + Control–MO
UUO + Snail1–MO1#5
H&E
Sirius Red
α-SMA
Vimentin
F4/80
pNFkB
c
Control–MO
Snail1–MO1#5
mRNA (fold change)
NL
L
Snai1
Snai2
Cadh1
Cadh16
Vim
Tgfb1
d
Cortical fibrosis (relative to Control–MO)
57%
Control MO
Snail1-MO#5
+ UUO

Figure 6

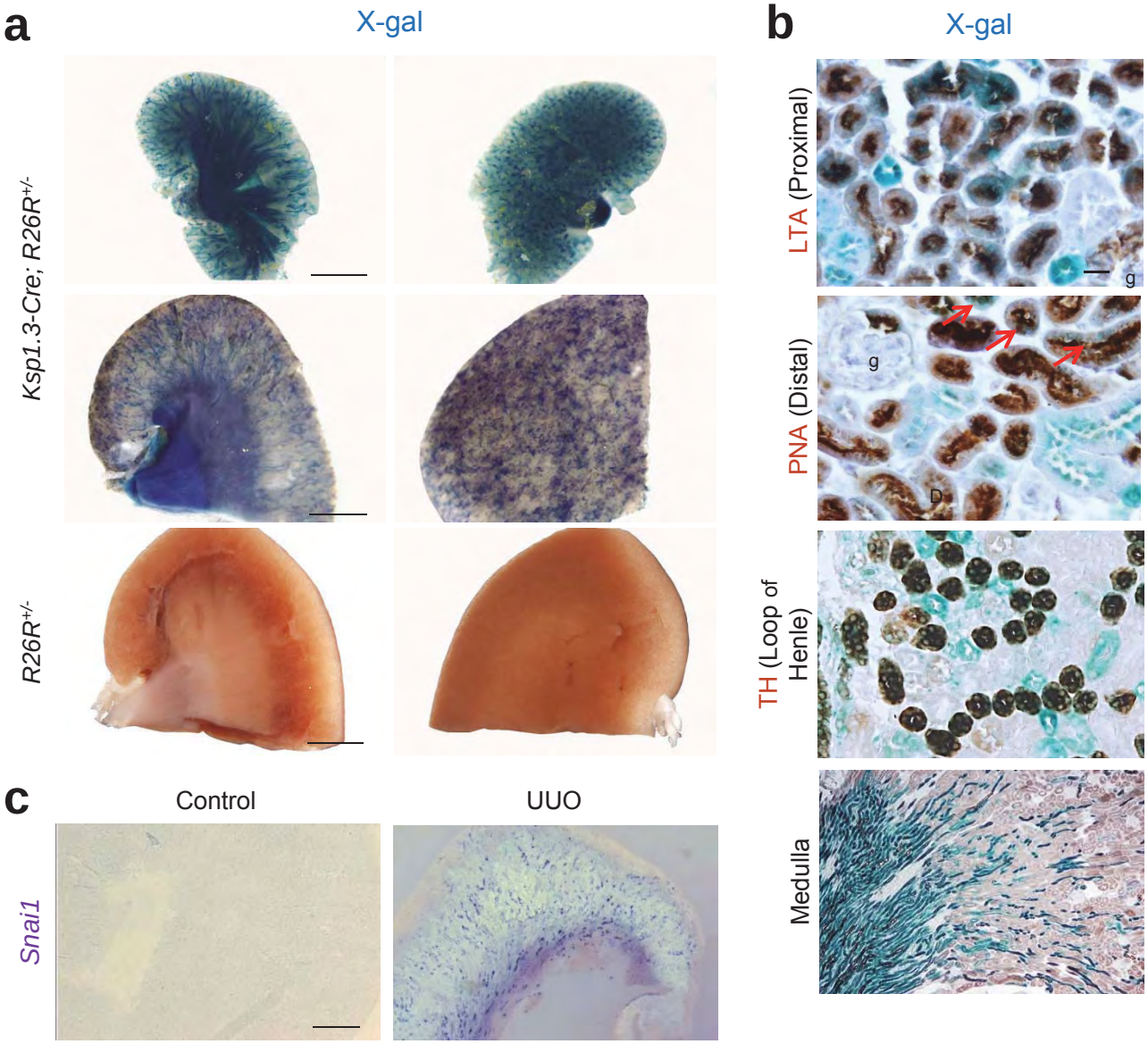

Supplementary Figure 1. Epithelial recombination mediated by *Ksp1.3-Cre* as assessed by crossing the mice with the Rosa26R (R26R) reporter strain. (**a**) Whole-mounted X-gal stained kidneys from *Ksp1.3Cre;R26R* newborn and adult mice (2-month-old) to detect β-galactosidase activity as an indication of Cre recombination. Recombination is detected in both kidney cortex and medulla. No staining is detected in kidneys from a transgenic mouse carrying only the *lacZ* reporter gene. Scale bars: 0.5 mm (top panel); 1 mm (middle panel and lower panel) (**b**) X-gal staining in sections obtained from *SFKC;R26R* kidneys and co-staining with different lectins, markers of proximal tubules (LTA) or distal tubules (PNA). Red arrows indicate examples of double positive tubules in the latter. Anti-Tam-Horsfall protein antibodies mark the thick ascending limb of Henle (TH), also stained for X-gal (β-galactosidase). X-gal staining is also prominent in the collecting ducts of the medulla. g indicates glomeruli. In summary, *Ksp1.3Cre* mediates recombination in collecting ducts, loop of Henle, the majority of proximal tubules and in some distal tubules. Scale bar: 20 μm (**c**) *Snai1* transcription is reactivated after UUO in both the cortex and the medulla. Control; sham-operated kidney. Scale bar: 1 mm.

Supplementary Figure 1

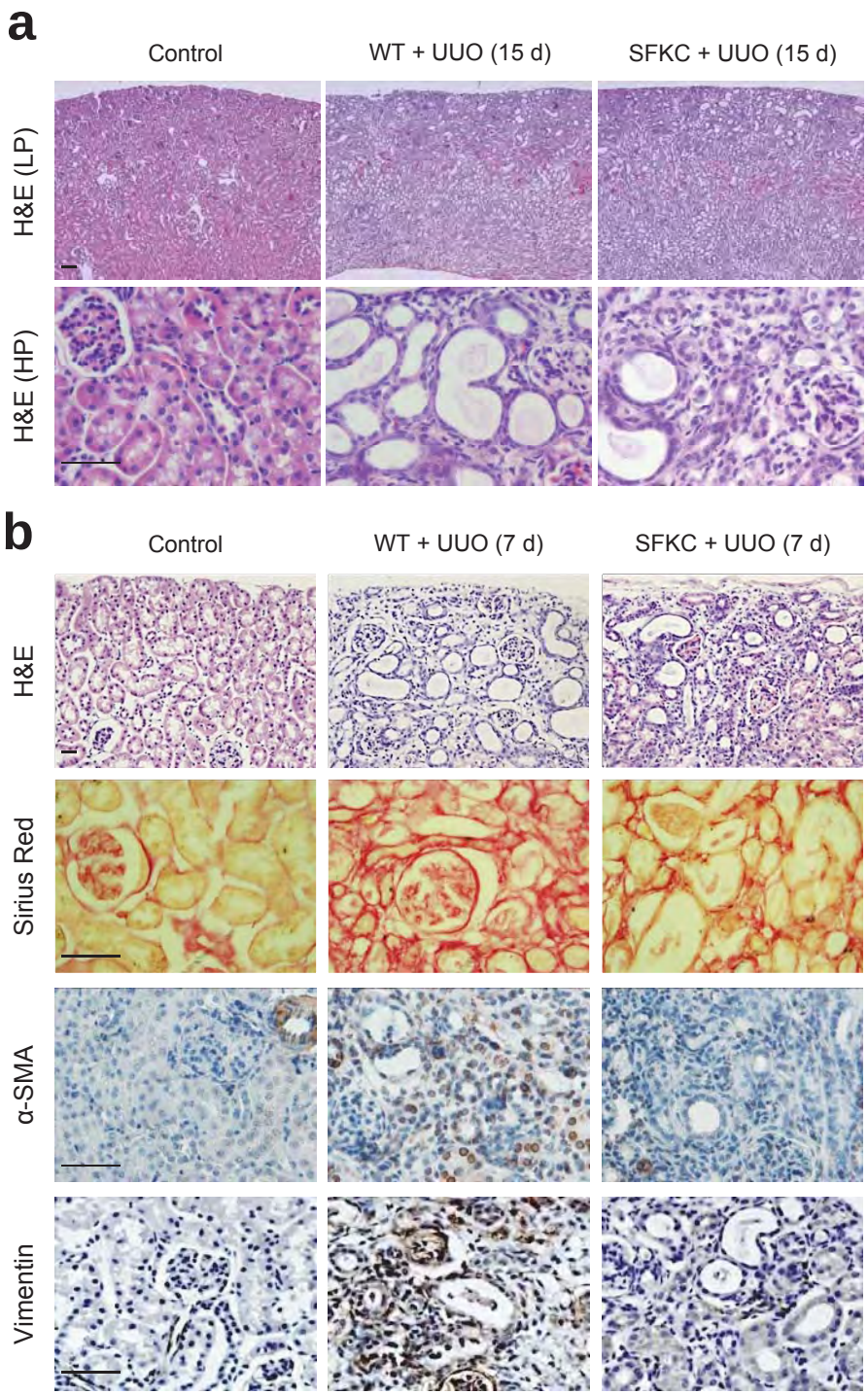

Supplementary Figure 2. (**a**) Low (LP) and high power (HP) images of H&E stainings in kidney sections similar to those shown in shown in Figure 1. (**b**) Kidney sections equivalent to those shown in Figure 1 but taken from sham-operated (control) and obstructed kidneys (UUO) of WT and SFKC mice 7 days after surgery. Tissue sections are representative of 8 independent samples examined from each of 6 mice per group. Scale bars: 50μm.

Supplementary Figure 2

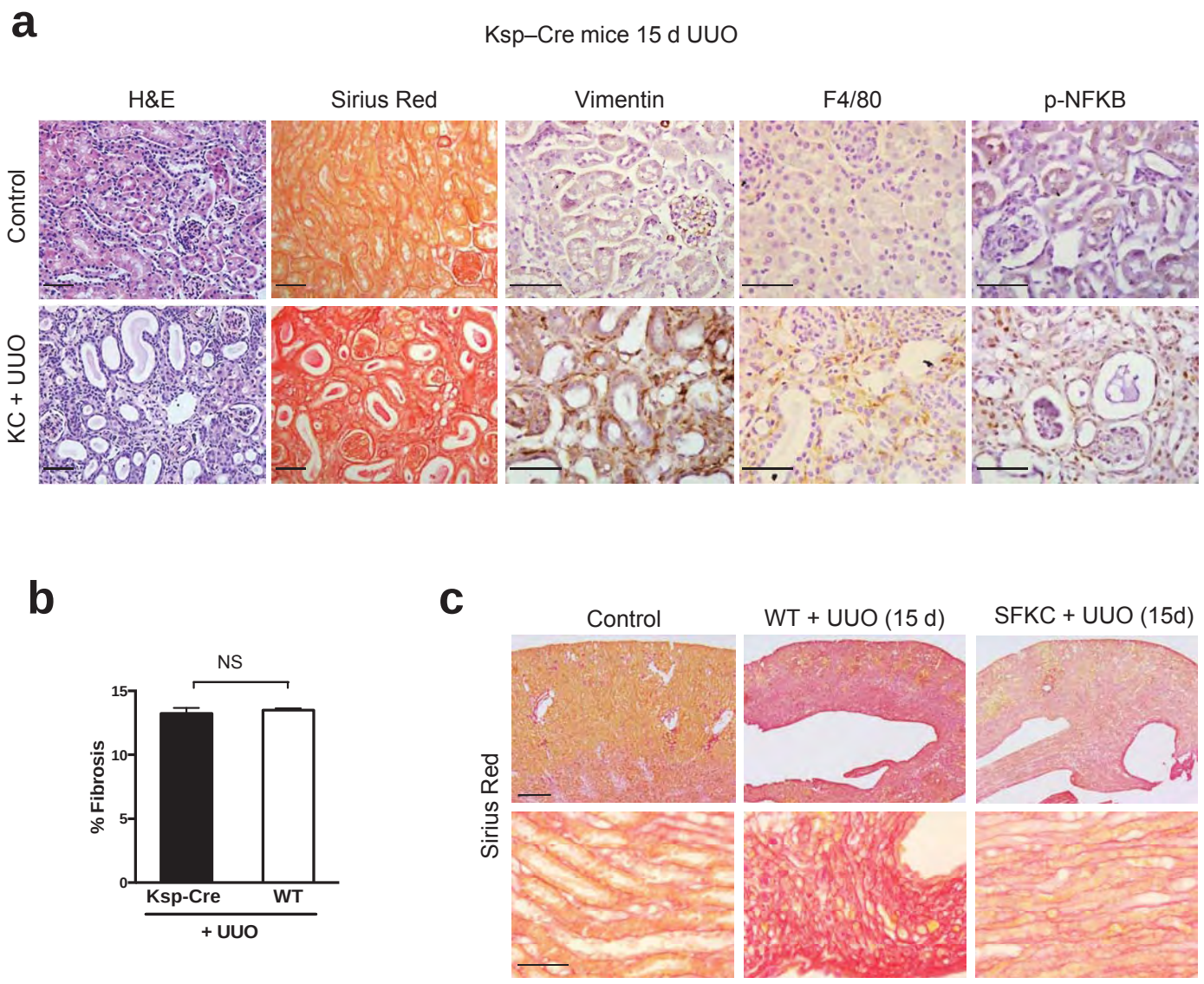

Supplementary Figure 3. (**a**) Kidney sections taken from sham-operated (control) and obstructed kidneys (UUO) of WT and Ksp1.3-Cre (KC) control mice 15 days after surgery. Tissue sections are representative of 3 independent samples examined from 3 mice per group. Scale bars: 50 μm. (**b**) Sirius Red quantification from obstructed kidney sections from WT and Ksp-Cre mice 15 days after surgery. Data represent the mean ± SEM of the % of the area occupied by collagen in 10 interstitial random cortical fields normalized to the area occupied by collagen in sham-operated controls from 3 mice per group. NS: non significant; Mann-Whitney test. (**c**) Sirius Red staining of sections taken from kidneys shown in Fig. 1. Upper panel, low magnification images. Lower panel, images of the medullar region of the same kidneys. Scale bars: upper panel 0.5 mm, lower panel 50μm.

Supplementary Figure 3

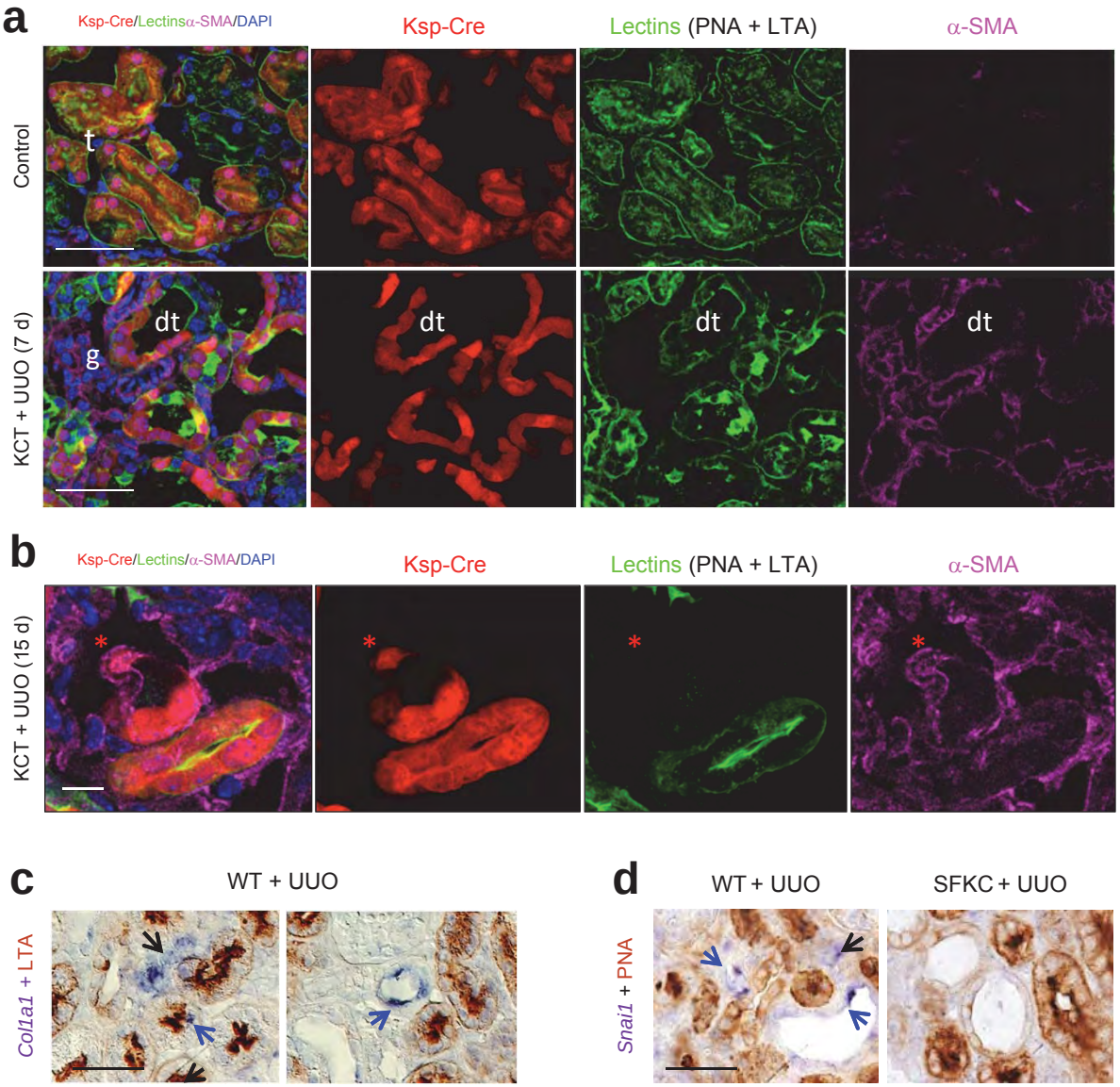

Supplementary Figure 4. (**a**) Ksp1.3-Cre; Tomato$^{fl/fl}$ mice (KCT) were subjected to UUO and kidneys were collected 7 days after surgery. Representative images (*n* = 10) from kidney sections from obstructed (KCT+ UUO) and contralateral non-obstructed kidneys (Control) stained for LTA and PNA (markers of proximal and distal tubules, respectively), α-SMA and counterstained for Dapi to visualize nuclei. Tomato fluorescent protein expression was directly visualized. dt, dilated tubule, g, glomerulus, t, tubule. (**b**) The field is selected to illustrate one of the rare tdTomato+ cells delaminating from the tubule (red asterisk), that has lost lectin expression. These cells represent less than 1% of tdTomato+ population. (**c**) *Col1a1* gene expression (blue, determined by in situ hybridization) and LTA (brown; immunohistochemistry) in kidneys from 8-week old wild type (WT) mice 7 days after UUO. *Col1a1* is transcribed after UUO in wild type mice in epithelial (blue arrows) and interstitial renal cells (black arrow). Tissue sections are representative of 6 independent samples examined. (**d**) PNA (brown, immunohistochemistry) and *Snai1* expression (blue, *in situ* hybridization). Snail1 is not induced in SFKC kidneys after UUO. Arrows indicate *Snai1* expression in the tubules (blue) and in the interstitial cells (black). Scale bars: 50μm.

Supplementary Figure 4

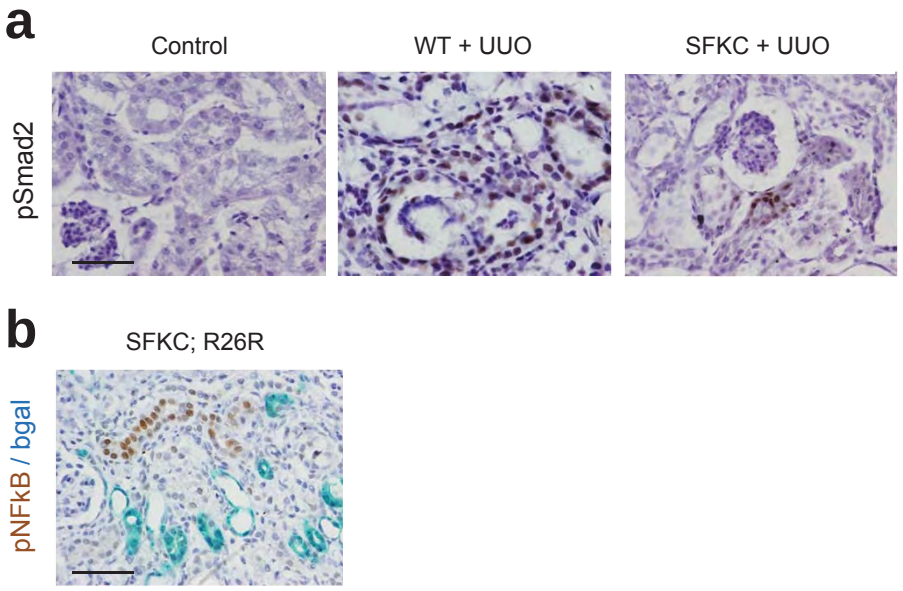

Supplementary Figure 5. (**a**) Phospho-Smad2 (pSmad2) stainings in representative sections (*n* = 5) from sham-operated (control) and obstructed kidneys (UUO) from WT or SFKC mice collected 15 days after surgery. (**b**) X-gal and pNF-κB (pNFkB) staining in obstructed kidneys from SFKC mice. Tissue sections are representative of 6 independent samples examined per mouse (n=6). Scale bars: 50μm.

Supplementary Figure 5

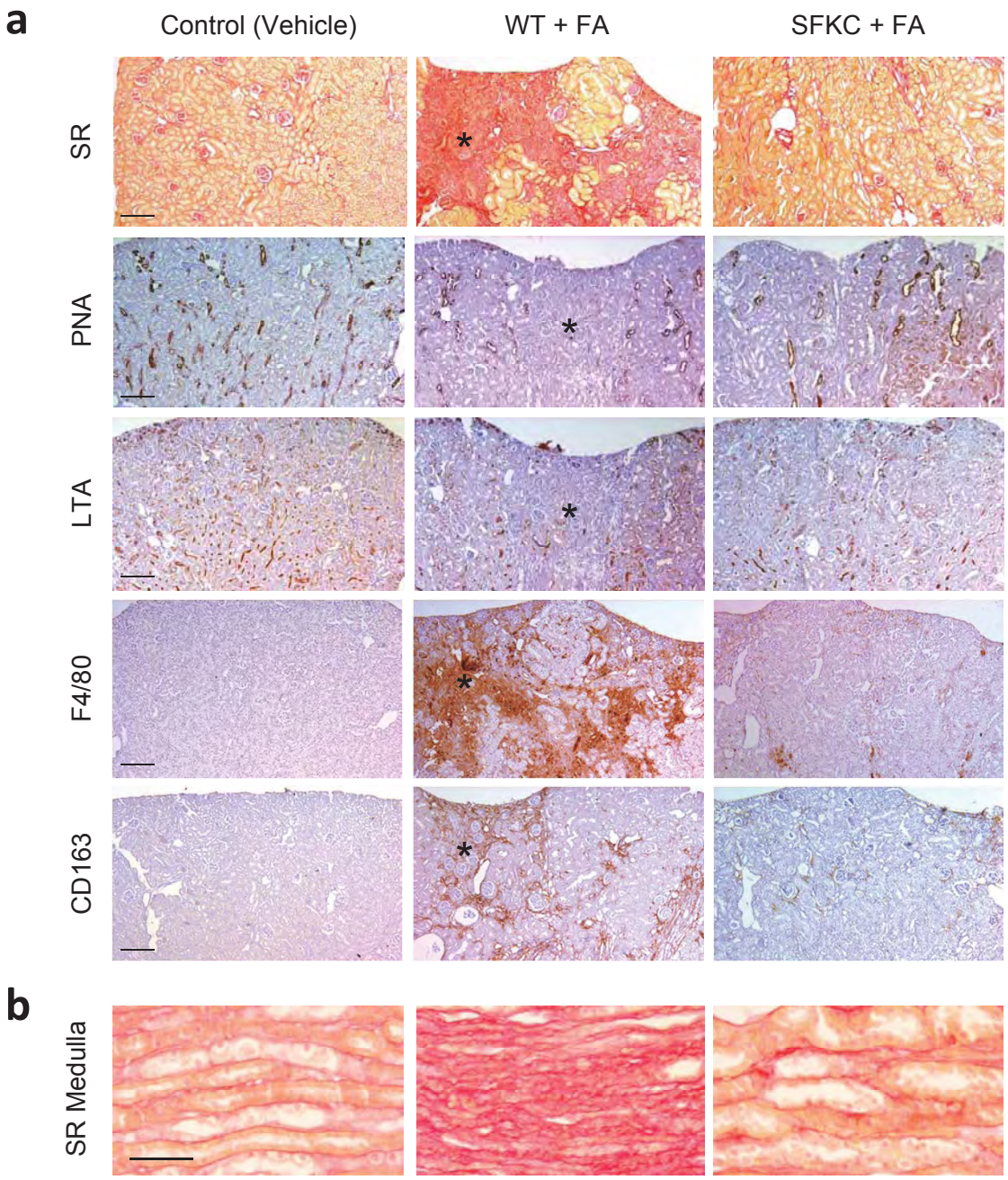

Supplementary Figure 6. (**a**) Low power magnification images of representative sections (*n* = 5) taken from kidneys shown in Fig. 4. Sections were taken from vehicle-treated WT (Control) and from FA-treated WT and SFKC mice (FA). Asterisks indicate fibrotic areas, patches where lectin expression (PNA and LTA, brown) is highly reduced and inflammation is high, as observed by the expression of F4/80 (macrophage marker) and CD163 (specific for M2 macrophages). Patches of healthy tissue observed as "crests" and fibrotic areas as "valleys". SFKC kidneys maintain lectin expression and show very much reduced macrophage colonization. Scale bars: 200 μm. (**b**) Representative images (*n* = 5) from Sirius Red staining of the medullar region from kidneys shown in Fig. 4. Scale bar: 50μm.

Supplementary Figure 6

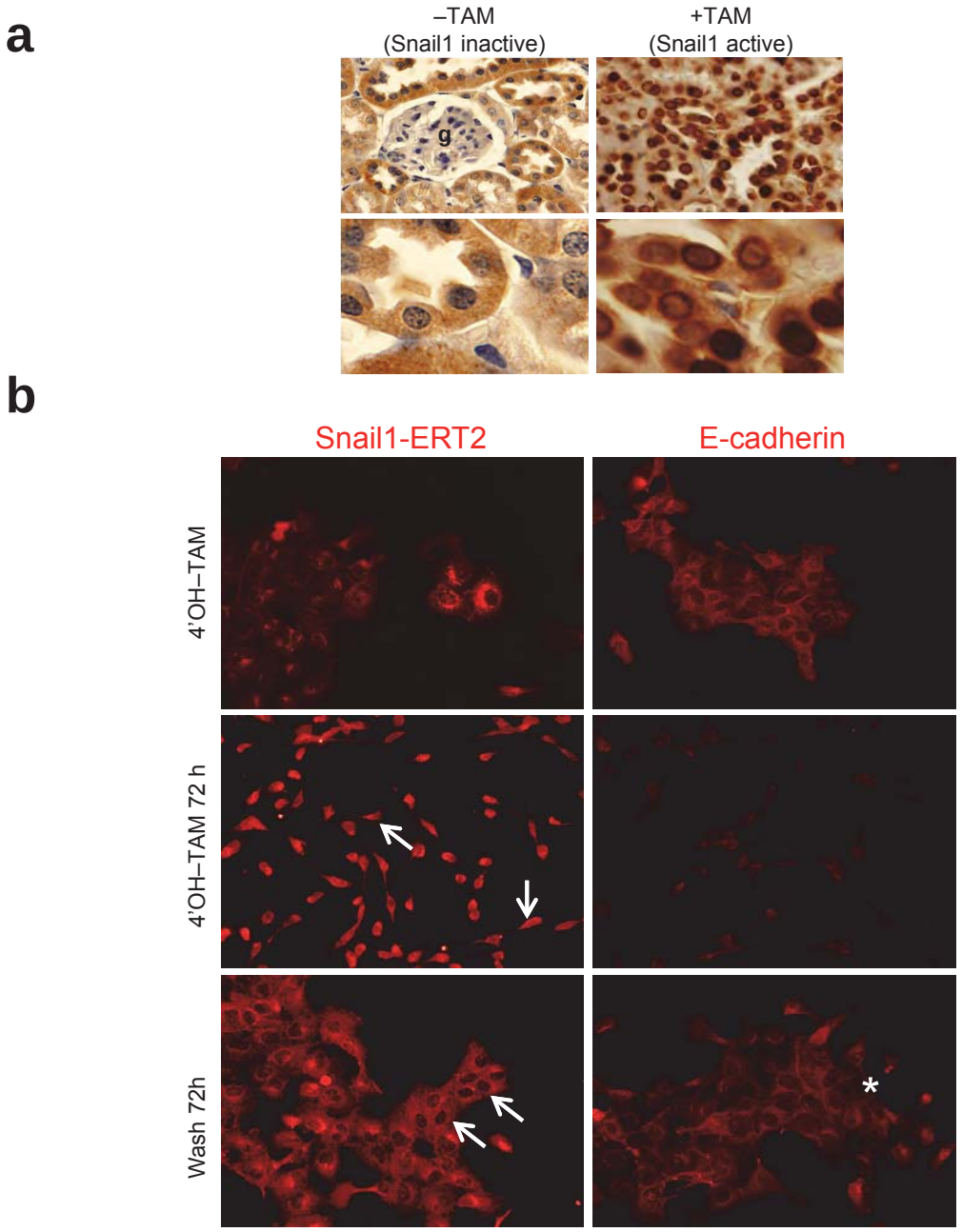

Supplementary Fig. 7. (**a**) Immunohistochemistry for the estrogen receptor showing exogenous Snail1 protein expression and activation upon tamoxifen treatment. Glomerular (g) and endothelial cells (arrows) are devoid of the transgenic protein. (**b**) MDCK cells (dog renal cells) were transfected with the Snail1 tamoxifen-inducible construct used to generate the Snail1-ERT2 transgenic mouse line. Middle panel: Cells were treated with 4-Hydroxytamoxifen (4'OH–TAM) for 72 hours and subjected to estrogen receptor and E-cadherin immunofluorescence analysis; arrows indicate Snail1 expression in the nucleus in cells that have adopted a mesenchymal phenotype. Bottom panel: cells were washed after 4'OH-TAM treatment and left in culture for an additional 72 hours period; arrows indicate Snail1-negative nuclei in cells with a epithelial morphology; Asterisks indicate recovery in E-cadherin expression.

Supplementary Figure 7

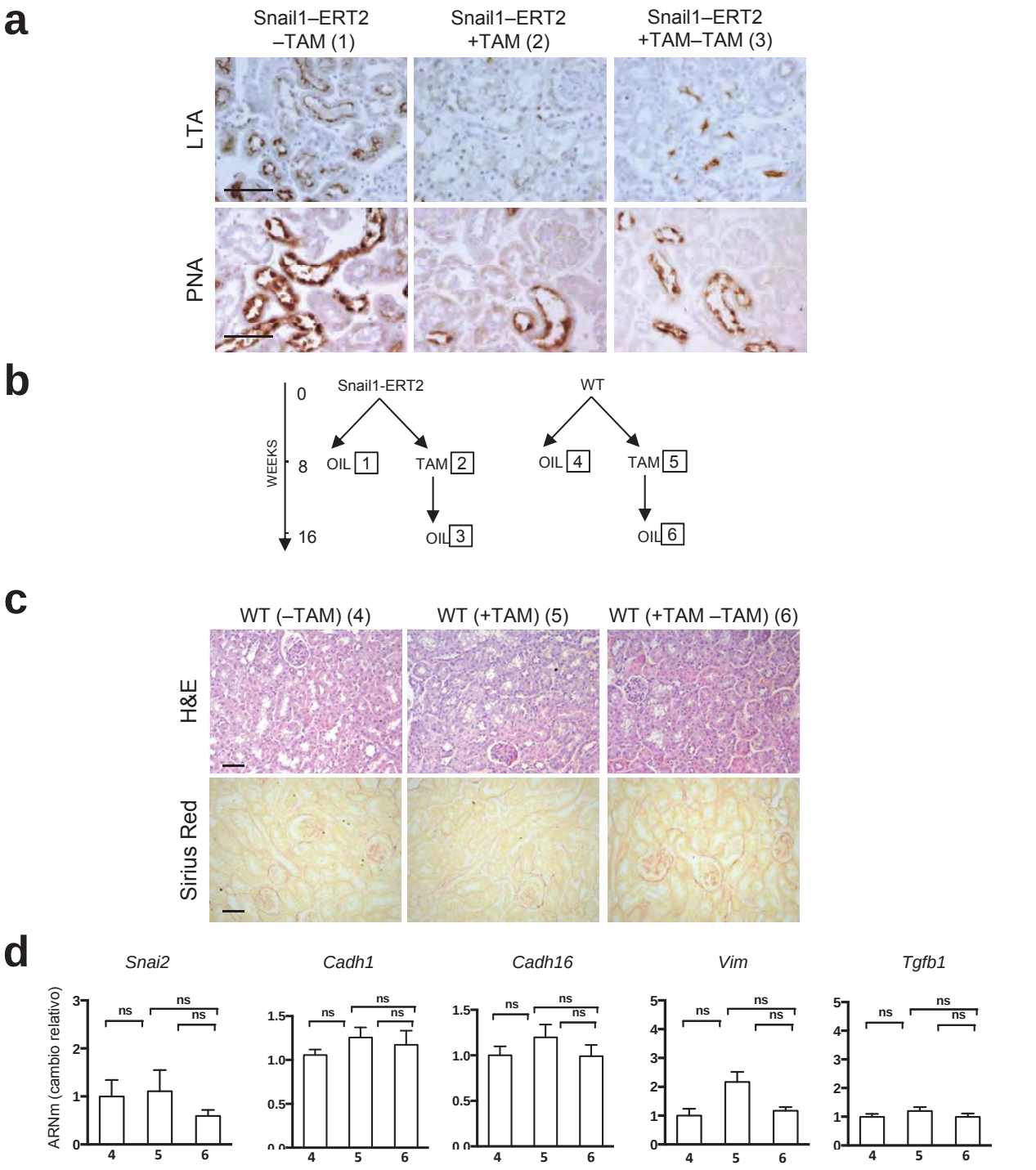

Supplementary Figure 8. (**a**) Expression of lectins (PNA and LTA) in kidneys from Snail-ERT2 mice subjected to the treatments shown in Figure 5. Scale bar: 50μm. (**b**) WT mice were treated with tamoxifen or corn oil (vehicle) in parallel to the treatments performed in Snail1-ERT2 mice shown in Fig. 5. (**c**) H&E and Sirius red stainings in 5 μm paraffin sections from kidneys from WT mice treated with corn oil (4), tamoxifen for 8 weeks (5), or tamoxifen for 8 weeks followed by oil treatment for another 8 weeks (6). Tissue sections are representative of 6 independent samples examined per mouse (n=4 per condition) Scale bar: 50μm. (**d**) *Snai2*, *Cadh1*, *Cadh-16*, *Vim* and *Tgfb1* mRNA levels detected by qRT-PCR in kidneys from WT animals in b. Data are normalized to vehicle injected kidney levels (4) and represent the mean ± SEM of groups of 3 mice; ns: non significant; One-way ANOVA followed by Tukey's multiple comparison test.

Supplementary Figure 8

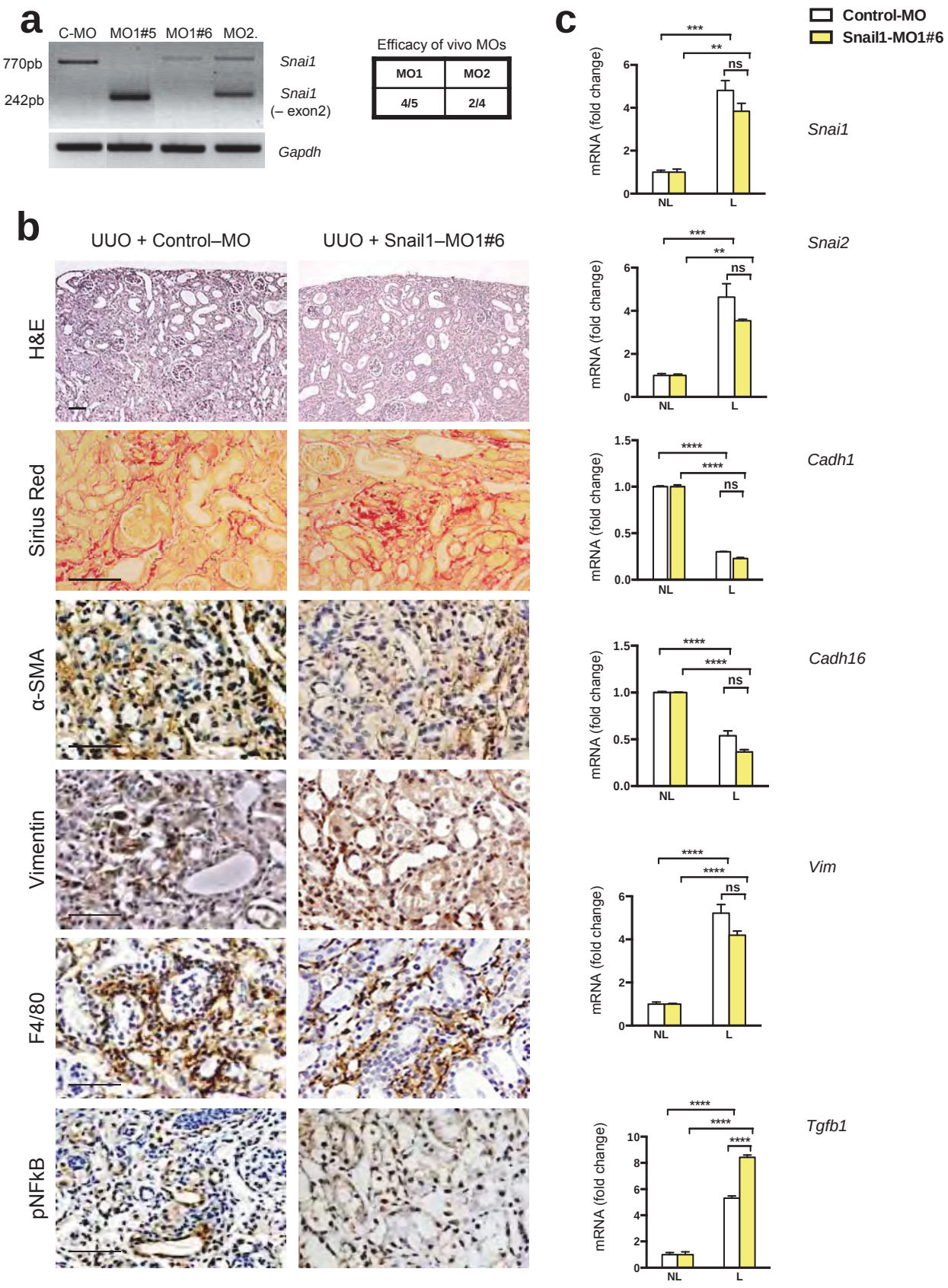

Supplementary Figure 9

Supplementary Figure 9. (**a**) RT-PCR analysis of *Snai1* transcripts expressed in obstructed kidneys from WT mice after treatment with Vivo-morpholinos designed to induce exon skipping in *Snai1* mRNA. The full-length product amplified from the normal transcript is 770 base pairs (bp), and the product missing exon 2 is 242 bp. Two VIVO-morpholinos (MO) were designed as described in Online methods. MO1 efficiently induced exon skipping in 80% of injected mice (4/5), while MO2 only partly worked in 2/4 injected mice. (**b** and **c**) Panels show data from mouse #6 in which MO1 did not work as assessed by its failure in inducing exon skipping (MO1#6, in **a**). Samples were treated as those from the mice in which MO1 effectively led to exon skipping (mouse #5; MO1#5 in **a**, and the corresponding data are shown in Fig. 6). (**b**) Representative images (n = 5) from hematoxylin-eosin (H&E) and Sirius red stainings, immunohistochemistry for mesenchymal markers (vimentin and alpha smooth muscle myosin; αSMA) and inflammation markers (F4/80 and phospho-NFkB (pNFkB)). (**c**) *Snai2*, *Cadh1*, *Cadh16*, *Vim* and *Tgfb1* mRNA levels detected by qRT-PCR in mouse #6. Data are normalized to contralateral non-obstructed kidneys (NL) and represent the mean ± SEM of triplicates (n = 5). $*P < 0.05$, $**P < 0.01$, $***P < 0.001$. Two-way ANOVA followed by Tukey's multiple comparison test. Scale bars: 50μm.

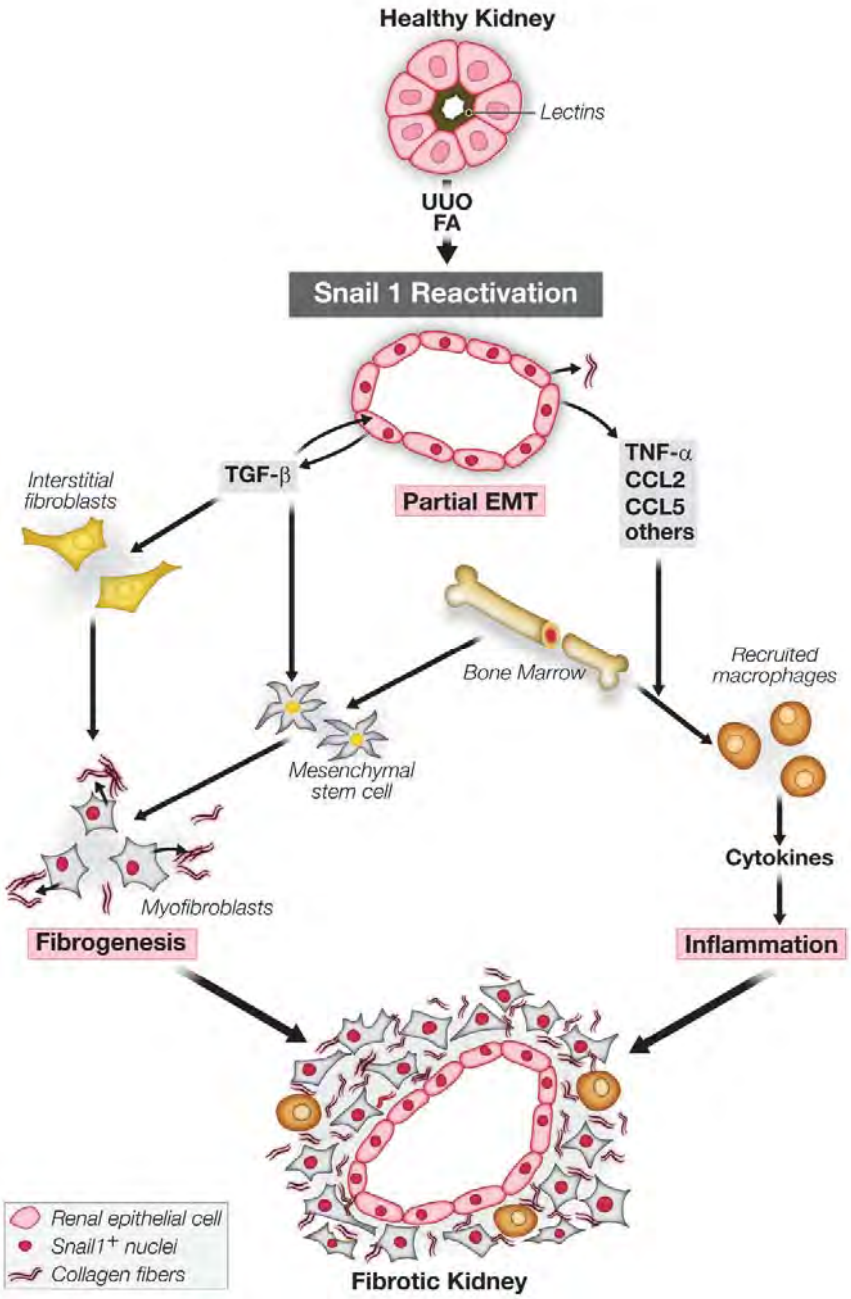

Supplementary Figure 10. Schematic representation of events downstream of Snail1 reactivation following unilateral ureteral obstruccion (UUO) or folic acid treatment (FA). Snail1 drives a partial EMT in kidney epithelial cells. Snail1–driven partial EMT promotes the dedifferentiation of tubular cells with the decrease in epithelial and polarity markers and the increase in mesenchymal markers. Importantly, epithelial cells remain integrated into the tubules while relaying fibrogenic and inflammatory signals to the interstitium which promote myofibroblast activation and the recruitment of immune cells.

Supplementary Figure 10

	-TAM (1)	+TAM (2)	+ TAM (16 w)	+ TAM – TAM (3)
Creatinine clearance (ml/min/100 g body weight)	1,25 ± 0,2	1,09 ± 0,56	0,9 ± 0,3 *	1,30 ± 0,2
Plasma creatinine (mg/l)	2,66 ± 0,5	3,26 ± 0,2	5,4 ± 0,7 *	2,48 ± 0,1

Supplementary Table 1. Creatinine clearance levels in ml/min per 100 g of body weight and plasma creatinine levels in mg/l from Snail1-ERT mice treated with vehicle (corn oil, –TAM (1)); tamoxifen for 8 weeks (+TAM (2)); tamoxifen for 16 weeks (+TAM 16w) and tamoxifen for 8 weeks followed by vehicle treatment for another 8 weeks (+TAM-TAM (3)). *p< 0.05; Mann-Whitney test.

Supplementary Table 1